HHS Public Access

Author manuscript

Adv Mater. Author manuscript; available in PMC 2018 June 01.

Published in final edited form as:

Adv Mater. 2017 June ; 29(23): . doi:10.1002/adma.201606857.

Cancer-Associated, Stimuli-Driven, Turn on Theranostics for Multimodality Imaging and Therapy

Xingshu Li, Dr.,

Department of Chemistry and Nano Science, Ewha Womans University, Seoul 120-750, Korea

Jihoon Kim, Dr.,

Laboratory of Molecular Imaging and Nanomedicine (LOMIN), National Institute of Biomedical Imaging and Bioengineering (NIBIB), National Institutes of Health (NIH), Bethesda, Maryland 20892, USA

Juyoung Yoon, Prof., and

Department of Chemistry and Nano Science, Ewha Womans University, Seoul 120-750, Korea

Xiaoyuan Chen, Prof.

Laboratory of Molecular Imaging and Nanomedicine (LOMIN), National Institute of Biomedical Imaging and Bioengineering (NIBIB), National Institutes of Health (NIH), Bethesda, Maryland 20892, USA

Abstract

Advances in bioinformatics, genomics, proteomics, and metabolomics have facilitated the development of novel anticancer agents that have decreased side effects and increased safety. Theranostics, systems that have combined therapeutic effects and diagnostic capabilities, have garnered increasing attention recently because of their potential use in personalized medicine, including cancer-targeting treatments for patients. One interesting approach to achieving this potential involves the development of cancer-associated, stimuli-driven, turn on theranostics. Multicomponent constructs of this type would have the capability of selectively delivering therapeutic reagents into cancer cells or tumor tissues while simultaneously generating unique signals that can be readily monitored under both *in vitro* and *in vivo* conditions. Specifically, their combined anticancer activities and selective visual signal respond to cancer-associated stimuli, would make these theranostic agents more highly efficient and specific for cancer treatment and diagnosis. This review focuses on the progress of stimuli-responsive turn on theranostics that activate diagnostic signals and release therapeutic reagents in response to the cancer-associated stimuli. The present article not only provides the fundamental backgrounds of diagnostic and therapeutic tools that have been widely utilized for developing theranostic agents, but also discusses the current approaches for developing stimuli-responsive turn on theranostics.

TOC image

Recent progress in the development of theranostic systems illustrates the future approach to highly specific and efficient cancer treatment. Novel and interesting theranostics, which can be

Correspondence to: Juyoung Yoon; Xiaoyuan Chen.

selectively turned on by cancer-associated stimuli, have been widely investigated. The results of this effort show the great promise of this approach in clinical applications. Particularly interesting are multimodal imaging guided therapy strategies that should play a special and meaningful role in personalized medicine.

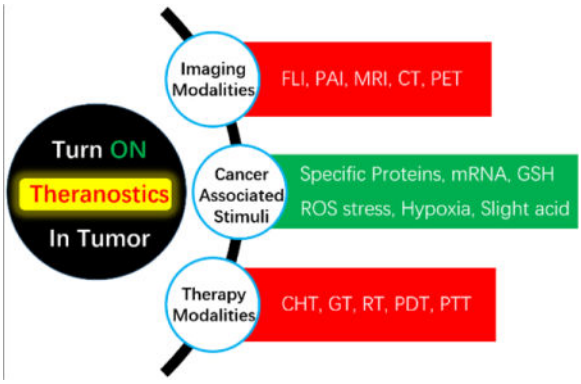

Keywords

theranostics; turn on; cancer anomalies; imaging modalities; targeting therapy

1. Introduction

Cancer is one of the most life-threatening diseases in the world. The GLOBOCAN series of the International Agency for Research on Cancer reported that the number of new cases of this disease in the world in 2012 was 14.1 million and the number of deaths caused by cancer in that year was 8.2 million.[1] The American Cancer Society estimated that the number of new cancer cases and deaths in the United States in 2016 will be 1,685,210 and 595,690, respectively.[2] The numerous advances that have been made in developing new technologies for cancer diagnosis and therapy have contributed to the continuous decline in the cancer death rate over several decades.[1,2] However, the limits of the current “one-size-fits-all” diagnostic and therapeutic strategies for treatment of this deadly disease has heralded the need for “personalized medicine” approaches.[3]

The aim of personalized medicine is to maximize therapeutic efficacy while minimizing side effects. One approach to this goal is to verify the patient’s genetic information and then conduct treatment with minimal delay after diagnosis.[4] While genotyping technologies such as the polymerase chain reaction (PCR) can be employed to identify genetic information and select treatment methods for individual patients, theranostics based strategies, which combine diagnosis and targeted therapy, can be utilized to treat the diseases and diagnose continuous changes in the patient’s disease state simultaneously. Therefore, theranostics are expected to realize the personalized medicine that enables to improve the pharmacokinetics, reduce the side effects and react immediately to the progress of diseases and conditions of patients by monitoring the therapeutic responses in real-time.[5]

Several considerations need to be addressed prior to designing appropriate agents that can be used for combined imaging based diagnosis and therapy. First, imaging and therapeutic

functions should be integrated into a single theranostic agent in order to minimize the time between diagnosis and therapy and to evaluate in real-time the prognosis after therapy.[5–9] Second, materials for theranosis should be carefully selected in terms of their biocompatibility and *in vivo* activity. Materials used for this purpose must be nontoxic and capable of displaying an imaging response *in vivo*. Third, theranostic agents should selectively accumulate in tumors and not in normal tissues in order to enhance the efficiencies of diagnosis and therapy. The active targeting strategy, based on the use of conjugating ligands that are capable of interacting with specific receptors overexpressed on target cells, has been widely utilized to enhance tumor localizing ability of agents used for diagnosis, treatment and theranosis.[10–13] Food and Drug Administration (FDA) approved antibody-drug conjugates (ADCs), including Adcetris® and Kadcyla®, exemplify the clinical potential of the active targeting strategy.[14] Another approach employs the passive targeting technique referred to as the “Enhanced Permeation and Retention (EPR)”, which allows macromolecules and nanomaterials to accumulate in tumors *via* leaky blood vessel that surround the tumor.[10,15] FDA approved Doxil®, Abraxane®, DaunoXome® and Marqibo® are representative examples that highlight the clinical potential of passive targeting.[6] In addition to these targeting strategies, red blood cell (RBC) membrane, CD47, sialic acid and polyethylene glycol (PEG) have been also investigated as methods to prevent non-specific tissue accumulation.[16–18] The fourth issue relates to the need for theranostic agents to exert both their therapeutic effects and diagnostic signals in response to targeted diseases. Efforts to identify cancer biomarkers that are specifically found in tumor microenvironments and inside cancer cells have led to methods for targeted delivery of therapeutic, diagnostic and theranostic agents.[19,20] A fifth consideration is that turn on strategies are generally preferred over their turn off counterparts owing to their lower background and high signal-to-noise (S/N) ratios in diagnosis directed imaging.[21,22]

Below, we discuss current progress that has been made in the development of cancer-associated, stimuli-driven, turn on theranostics that address the aforementioned issues. Before focusing on these efforts, we provide a brief introduction of materials for multimodal imaging and therapy that have been widely used in the development of theranostics as a background for understanding and appreciating the subsequent sections. In addition, perspectives and challenges of the use of stimuli-driven, turn on theranostics for cancer therapy are discussed at the end of the review.

2. Multimodal Imaging and Cancer Therapy

2.1. Multimodal Imaging

In vivo imaging techniques are required not only to diagnose cancers and identify the heterogeneity of tumors, but also to monitor the constantly changing disease states of patients.[23] Accordingly, several imaging tools have been developed and exploited for clinical and/or preclinical purposes, such as optical fluorescence (FLI), ultrasound (US), magnetic resonance imaging (MRI), computed tomography (CT), single photon emission computed tomography (SPECT), positron emission tomography (PET), and photoacustic imaging (PAI).[23–25] In this section, we briefly introduce the strengths and limitations of

each of these imaging modalities and the imaging probes employed for each modality (Table 1).

FLI involves detecting light emission of fluorophores promoted by absorption of light at specific wavelengths.[23,24,26] For *in vivo* applications, near-infrared (NIR) fluorophores have been developed to enhance deep tissue penetration and prevent interference associated with scattering and auto-fluorescence caused by tissues as well as biomolecules.[26–31] Representative fluorophores with NIR absorption characteristics include small organic dyes,[26–28] quantum dots (Q-dots)[29,31] and upconversion nanoparticles (UCNPs).[30,31] Compared to other imaging modalities, the FLI technique is non-invasive, relatively inexpensive and simple to perform. These characteristics facilitate multicoloar detection by simultaneously using several fluorophores.[23,26,31] However, spatial resolution and deep tissue penetration limitations still exist.

US is a non-invasive, inexpensive and fast imaging modality that can be employed in real-time.[23,32–34] When high-frequency sound waves passing through a body encounter boundary of tissues, a portion are reflected back to the probe. The intensities and distances of the sound wave echoes can be used to locate internal organs and body structures. Although sound waves themselves can be utilized for *in vivo* imaging, the presence of echogenic particles (contrast agents) enhances the accuracy of diagnoses.[33,34] Commercialized contrast agents for US include Albunex® (albumin shell with air), Optison™ (albumin shell with octafluoropropane), Definity® (lipid/surfactant shell with octafluoropropane), Imagent® (lipid/surfactant shell with N_2/perfluorohexane), Sonovue® (lipid shell with sulphur hexafluoride) Levovist® (lipid/galactose shell with air) CARDIOsphere® (PLGA polymer/albumin with N_2) and Sonovist® (cyanoacrylate polymer shell with air).[34] In addition, a number of nanoparticles as well as microparticles that have the ability to generate gases have been developed for target specific US imaging.[33,35–39] However, applications of US are limited by low resolution, dependency on skilled operators and difficulties in obtaining information about organs containing gas or behind bones.

Since the discovery that paramagnetic ions affect proton relaxation rates, MRI has become the most widely used diagnostic tool owing to its high spatial resolution and unlimited tissue penetration.[23,24,40,41] In MRI, a radio-wave radiation pulse at the resonance frequency of a nuclei induces nuclear spin transitions which cause equal populations of high and low energy nuclear spin states. Following the pulse, equilibration occurs to create a normal Boltzman distribution (T_1 relaxation) of the spin states and phase coherence is lost from nuclear spin vectors (T_2 relaxation). MR contrast imaging can be obtained by measuring these relaxation times.[42] As paramagnetic species including Mn^{2+}, Mn^{3+}, Cu^{2+}, Fe^{3+}, and Gd^{3+} significantly reduce the relaxation times, their target specific accumulation facilitates concentration-dependent MR contrast imaging and diagnosis.[41,42] In addition, superparamagnetic iron oxide nanoparticles are also employed as T_2 contrast agents owing to the susceptibility effects of the core of iron oxide.[43,44] Although numerous MR contrast agents have been developed and used for clinical diagnosis,[45–48] the disadvantages of this modality are its low sensitivity, time-consuming use and high cost.[23,41]

CT is a non-invasive modality that is used to obtain three-dimensional images of tissues of interest. This technique relies on processing of X-ray images taken from different angles using software programs.[23,24,49–51] Because electron dense structures improve the X-ray attenuation, CT itself can be utilized to detect hard tissues including bones.[50,51] However, it is challenging to get information of soft tissues or interface between two adjacent tissues by using CT alone. CT contrast agents increase the absolute CT attenuation, which facilitate the differentiation between normal tissue and tissue of interest when they are selectively delivered to target sites.[50] Various CT contrast agents based on iodinated compounds and barium sulfates have been clinically exploited, and nano-formulations containing iodinated compounds, lanthanide nanoparticles, gold nanoparticles (AuNPs), tantalum nanoparticles and bismuth-based nanoparticles are under development.[49–51] Although CT has advantages associated with fast diagnosis, high spatial resolution and unlimited depth penetration, it has potential side effects caused by radiation and contrast agents.[52,53]

Both SPECT and PET are radionuclide and γ-ray based techniques used for *in vivo* imaging.[23,24,54–56] The differences in these methods are associated with differences in radionuclides and detection systems.[54–56] SPECT generally utilizes ^{123}I, ^{99m}Tc, ^{111}In, ^{67}Ga, and ^{201}Tl that directly emit γ-rays, while PET uses nuclides including ^{11}C, ^{13}N, ^{15}O, ^{18}F, ^{64}Cu, ^{68}Ga, ^{76}Br, and ^{124}I that emit positively charged particles (positron). In PET, an emitted positron annihilates a nearby electron to produce two γ-rays. Because the half-lives of nuclides used for PET are in the range of minutes to hours, the cyclotron utilized to generate radionuclides for PET must be close to the PET facility. In contrast, radionuclides for SPECT have relatively long half-lives ($t_{1/2}$=hours to tens of hours) compared to PET,[54] which not only makes SPECT more economical than PET but also serves as the reason why SPECT can be used for long term studies. Moreover, whereas the gamma ray detector in PET directly records information arising from the paired γ-rays produced, SPECT requires a collimator in front of the gamma detector, which causes a lower detection efficiency than PET. Both PET and SPECT are more sensitive than MRI, and PET is known to have the highest sensitivity among all of the *in vivo* imaging techniques. However, radiation risks are major drawbacks of both techniques.

PAI is a distinctive diagnostic tool that utilizes a pulsed laser as an energy source and ultrasonic waves as signals.[25,57–59] When a pulsed laser beam encounters tissues and *in vivo* components including hemoglobin, melanin, lipid, and myoglobin, the light energy is changed to heat (called a photothermal effect) and the temperature of the targeted region increases. This results in thermo-elastic expansion that generates ultrasonic waves. As photoacoustic signals produced by intrinsic *in vivo* components are not sufficient to visualize and distinguish diseases, PAI contrast agents with high photothermal coefficients have been developed. These agents include fluorescent proteins, indocyanine green, evans blue, methylene blue, coomassie blue, prussian blue, AuNPs, silver nanoparticles (AgNPs), copper sulfide nanoparticles (CuS NPs), iron oxide nanoparticles, Q-dots, carbon-based materials and semiconducting polymers. PAI gives high contrast and resolution because it is based on optical absorption and ultrasonic detection. However, many barriers exist in utilizing this technique, including low sensitivity, limited tissue penetration and difficulty in detection of tissues blocked by bones or air cavities.

As discussed above, each imaging modality has its inherent pros and cons and some intrinsic limitations are difficult to circumvent. Accordingly, multimodal imaging methods that combine two or more of these modalities such as PET/CT and PET/MRI[23] have attracted significant attention. Agents that be utilized for multimodal imaging are currently under development.

2.2. Multimodal Therapy

Surgery, chemotherapy (CHT) and radiotherapy (RT) are widely utilized clinical methods to treat cancer. In particular, surgery is a practical approach to treat cancers that are in locations that are easy to detect and access. However, surgery is not effective for tumors that are too small to distinguish and those that have metastasized to multiple tissues. As a result, combination therapies have been employed to enhance the therapeutic efficacy, such as surgery/radiotherapy, surgery/chemotherapy, radiotherapy/chemotherapy, and surgery/radiotherapy/chemotherapy. These approaches, which utilize a combination of two or more therapeutic modalities to maximize the curative value and are classified as multimodal therapies, are widely used in the practical treatment of tumors. Herein, we briefly introduce the characteristics and challenges of therapeutic modalities that are not only currently used in the clinic but also those that are under development, such as CHT, gene therapy (GT), RT, photodynamic therapy (PDT) and photothermal therapy (PTT).

In CHT, small chemical compounds are utilized to kill tumors by interfering with processes such as transcription, cell division and DNA replication. Chemical drugs in CHT generally include doxorubicin (DOX), paclitaxel, camptothecin (CPT), 7-ethyl-10-hydroxycamptothecin (SN-38), S-crizotinib, gemcitabine and etoposide, etc. Numerous drug delivery systems, including nanoparticles and antibody-drug conjugates (ADC) platforms, have been developed to enhance the therapeutic effects of CHT by improving bioavailability and tumor targeting efficacy of drugs. Several drug delivery systems, such as Doxil®, Abraxane®, DaunoXome®, Marqibo®, Adcetris® and Kadcyla® have been successfully translated into clinical use. [6,14] Most drug delivery systems exploit passive and/or active targeting strategies to enhance the delivery efficiencies of drugs and the resultant therapeutic effects. In addition, current efforts focus on methods to evade non-specific delivery of drugs by optimizing the size, surface charge and surface chemistry,[17,60] and to control drug release by using stimuli-responsive moieties.[61–66]

GT is an approach to treating diseases by delivering therapeutic nucleic acids that alter the transcription or translation of DNA or RNA.[67–71] As part of studies of this fundamentally new treatment mode, numerous viral and non-viral gene delivery systems are under development. These delivery systems are needed because intact nucleic acids are easily degraded before reaching target sites and are difficult to transfect into cells due to their negative charge and large size characteristics. Adenovirus, adeno-associated virus, retrovirus and lentivirus are useful viral vectors, which have been shown to have high transfection efficiencies. However, immune responses and unintended mutagenesis of host cells caused by these modified viruses are significant issues that need to be considered prior to their practical applications.[67,68] Non-viral vectors for this purpose are typically cationic polymers including polyethyleneimine, poly(L-lysine), and chitosan. Despite the ease of

their functionalization and their elicitation of relatively lower immune responses compared to viral vectors, non-viral vector have limitations associated with phagocytic elimination, high cytotoxicity and low transfection efficiency. As a result, studies are underway to develop novel gene delivery carriers that utilize neutral charged polymers and inorganic nanoparticles to alleviate the non-specific cytotoxicity, enhance transfection efficiency and confer multifunctionality.[67,69–71] As is the case with drug delivery systems, stimuli-responsive gene delivery systems have also received significant attention as part of target-specific efficient gene therapies.[72]

RT is a method to treat tumors by using high-energy radiation including X-rays and γ-rays (external-beam RT) and/or by delivering radionuclides to the cancer cells (internal RT).[73–76] In contrast to external-beam RT, which utilizes an linear accelerator,[73,74] the therapeutic potential of internal RT highly depends on the accumulation of radionuclides in the target sites. Radionuclides can be directly delivered to tumors *via* catheters, and tubes or needles if tumors are located in easily accessible sites.[75] However, radionuclides need to be selectively delivered to tumors *via* systemic pathways when they are not accessible.[76] Targeted delivery systems for radionuclides are continuously being developed to achieve efficient cancer therapy while minimizing non-specific cytotoxicity.[76]

PDT[77–81] and PTT[67,82–86] use the conversion of light energy to chemical and thermal energy, respectively, to kill tumors. PDT is carried out by light irradiation of photosensitizers such as chlorins, purpurins, bacteriochlorins, phtalocyanine, napthalocyanine, and indocyanine green. This process results in the generation of reactive oxygen species (ROS) that contribute to PDT-induced death of cancer cells and induction of anti-tumor immune response.[77–81] Because photosensitizers generally exhibit poor water solubility, hydrophilic functional groups are typically introduced for therapeutic purposes. In addition, nanoparticles such as polymeric nanoparticles, AuNPs and Q-dots are used together with photosensitizers to surmount this issue.[81] In terms of PTT, template materials such as AuNPs, silver nanoparticles (AgNPs), carbon nanotubes, graphene derivatives, single layered transition metal dichalcogenides (TMDCs), black phosphorus, indocyanine green, and melanin derivatives with high photothermal conversion efficiencies are utilized to perform light induced tumor destruction.[67,82–86] These two modalities constitute spatio-temperal controlled therapy which avoids systemic cytotoxicity because the site and time of light irradiation can be tuned by an operator. However, targeted accumulation of PDT or PTT agents is required to reach the full therapeutic potential of these methods because their activities are highly dependent on light-converting efficiencies and concentrations. Furthermore, it is noteworthy to mention that the use of agents with NIR windows is a prerequisite for deep delivery of light energy to tumors.

We do not intend to discuss each therapy, more comprehensive reviews for CHT, GT, RT, PDT and PTT can be found in ref. 64, 69, 76, 78 and 83. Recently, multimodal therapies using combinations of CHT, GT, PDT and PTT have been investigated. In addition, multimodal therapy has been amalgamated with multimodal imaging in order to bring about the potential for theranostics. The current stage and challenges of stimuli-responsive theranostics will be discussed in the following sections.

3. Examples of Cancer-Associated Stimuli-Driven Turn on Theranostics

3.1. Specific Protein-Driven Turn on Theranostics

Proteins are important and indispensable biomacromolecules in living organisms. It is known that abnormal expression of proteins are usually related to diseases. In cancer, there are protein biomarkers that are either expressed by tumor cells themselves or by other cells (e.g. tumor associated macrophages, stromal cells, etc.) involved in cancer.[87] Most protein biomarkers associated with cancer serve diversified clinical purposes during early or late stages of the disease. As a result, these biomarkers can be utilized to monitor responses to cancer treatment and/or to probe recurrence or progression after treatment.[88] Recently, several activatable designs such as hairpin peptide beacons, supramolecular approaches, aggregation-induced emission (AIE), and structure-switching aptamers have been utilized to probe cancer-associated protein biomarkers and deliver therapeutic agents. Visualizing signals and/or anticancer activities can be turned on upon recognition of the targeted proteins through affinity labeling, recognition of specific peptide fragments, electrostatic interaction or hydrophobic ligand-binding. In Table 2 are summarized specific protein-driven, turn on theranostics that have been reported in recent years. The protein responsive linkers/groups, signal output units, therapeutic activity units, and imaging and therapeutic modalities are also given in this table.

3.1.1. Enzyme-Driven Turn on Theranostics—Enzymes are biologically catalytic, diverse and vital to almost all metabolic processes in cells because they promote more than 5,000 biochemical processes.[106] Because a small number of enzyme molecules can continually and effectively bring about theranostic activation, high levels of signal amplification are expected. Accordingly, enzymes are promising targets for the development of activatable theranostics. Below, we described recent progress made in studies of enzyme-activated theranostics, including cathepsin B-, hyaluronidase (HAase)-, matrix metalloproteinases (MMPs)-, NAD(P)H:quinone oxidoreductase-1 (NQO1)-, protein tyrosine kinase-7 (PTK7)-, and caspases-activated strategies.

Cathepsin B: Cathepsin B belongs to a family of lysosomal proteases that promote intracellular proteolysis. Because overexpression of cathepsin B is relevant to invasiveness and metastasis, it is a potential biomarker for many types of cancers, such as breast cancer and pancreatic cancer.[107,108] A peptide bearing a Gly-Phe-Leu-Gly- (GFLG) unit, which is selectively cleaved by cathepsin B, has been utilized for enzyme-responsive imaging and drug delivery.[108]

In 2014, Kim *et al.* described a cathepsin B activatable porphyrin based photosensitizer.[89] In this system, chlorin e4 (Ce4) was conjugated through a cathepsin B cleavable RRK peptide linker with a folic acid (FA) group, which serves as an efficient quencher of the porphyrin excited state. This smart dual-targeting theranostic agent shows strong fluorescence emission and promotes photocytotoxicity only after the RRK linker is cleaved by cathepsin B in folate receptor-positive cancer cells. The results of *in vitro* and *in vivo* studies show that this activatable photosensitizer can be used for dual-targeting NIR FLI and cancer-selective PDT.[89]

One year later, Yuan *et al.* described an aggregation-induced emission (AIE) fluorogen/photosensitizer that can be used for cathepsin B activatable FLI and PDT.[90] This bioprobe is comprised of four functional components including an AIE fluorogen for both imaging and PDT, a cathepsin B responsive GFLG peptide, a specific tri-aspartic acid (D) linker for improved hydrophilicity, and a cyclic arginine-glycine-aspartic acid (cRGD)-targeting group. The probe in aqueous solution is in a fluorescence turn-off state and it promotes only low levels of ROS production. These characteristics are a consequence of excitonic energy consumption caused by intramolecular motion. However, its aggregate formed by cathepsin B mediated cleavage of the GFLG peptide efficiently fluoresces and is photocytotoxic. This finding shows the desirable potential of this single bioprobe for use in tumor-targeting imaging and therapy.[90]

HAase: HAase is a family of endoglycosidases that catalyze hydrolysis of hyaluronic acid (HA). HAase is overexpressed in a variety of cancer cells, including malignant melanoma carcinoma, bladder carcinoma, prostate carcinoma, and so on.[109–111] Consequently, it has become a new biomarker for early diagnosis and therapy of cancer.

In 2013, Choi's group reported that a graphene oxide (GO)-chlorin e6 (Ce6) complex serves as a HAase activatable theranostic agent for FLI and photo-induced A549 human lung cancer cell inhibition.[91] In this system, HA coupled with Ce6 is loaded on the surface of GO through physical adsorption. Because of the efficient quenching ability of GO, fluorescence emission and singlet oxygen ($^1O_2$) production of Ce6 are strongly inhibited. However, HAase hydrolytically cleaves the polymer backbone of HA which releases Ce6 from the GO. This process results in the development of strong fluorescence emission and light irradiation induced $^1O_2$ generation. Additionally, the strong surface plasmon absorption of GO enables it to be a good photothermal agent for NIR mediated PTT.[91]

In 2015, Huang *et al.* developed a HA/conjugated polymer-DOX complex that can be used to detect HAase selectively and deliver an anticancer drug.[92] The cationic conjugated polymer (PEEP) in this complex is non-fluorescent because of quenching by electron transfer from PEEP to DOX (Figure 1). However, HAase promotes hydrolysis of HA which results in release of DOX. As a result, the fluorescence of PEEP is recovered to a degree that is dependent on the concentration of HAase. Because this method has a detection limit of 0.075 U/mL, it is applicable for rapid and reliable HAase detection. In addition, owing to the specific affinity of HA with CD44 receptors, this system was employed for Hela cells targeted drug delivery.[92]

Very recently, Shi *et al.* developed a HAase-activated theranostic for activatable PDT and simultaneous cancer (HCT-116 cancer cell line) diagnosis that is based on diiodostyryl-bodipy conjugated HA nanoparticles (DBHA-NPs).[93] The quenching and restoration of photoactivity of this system is controlled by self-assembly of diiodostyryl-bodipy in aqueous solution and its disaggregation promoted by HAase in cancer cells.[93]

MMPs: MMPs are calcium-dependent, zinc-containing endopeptidases that belong to the metzincin superfamily. MMPs are known to play an important role in tissue remodeling in a variety of physiological and pathological processes including cancer invasion and

metastasis. As a result, MMPs have great potential in cancer diagnosis and targeted therapy owing to their overexpression in many kinds of cancer cells compared to healthy counterparts.[112,113]

In 2016, Gao *et al.* developed the multifunctional theranostic probe CPGA for MMP-14 sensitive dual modal fluorescence and PA imaging guided PTT.[94] This theranostic probe consists of a GO and Au nanocomposite (GA) covalently conjugated with a Cy5.5 labelled GATRLFGIRG peptide (Figure 2). As a result of a surface plasmon resonance effect from Au to Cy5.5 and fluorescence resonance energy transfer between Cy5.5 and GO, the excited state of Cy5.5 is quenched to the extent of 95%. However, fluorescence emission returns after degradation of the GATRLFGIRG peptide induced by MMP-14. On the other hand, loading Au nanoparticles with a uniform diameter of about 15 nm on the surface of GO causes it to have an enhanced photothermal conversion efficiency because of its stronger NIR absorption. At a low light levels (808 nm, 0.3 W/cm^2, 10 min), this nanohybrid displays a significant temperature increment with a value of $\Delta T = 23$ °C that is much higher than that of either GO or Au alone. The excellent photothermal properties of the nanocomposite not only facilitate PAI, but also enable absolute abolition of tumors in SCC7-bearing mice under light irradiation. This nanocomposite, which has the ability to function in FLI, PAI and PTT, is a highly promising specific enzyme-sensitive theranostics.[94]

In the same year, Zhang and his coworkers described a MMP-2 activated theranostic nanoplatform for both FLI and anticancer drug release.[95] This system is based on mesoporous silica nanoparticles (MSNs) loaded with CPT whose surface is coated with cRGD targeting units and MMP-2 activatable probes comprised of a fluorophore, MMP-2 sensitive GPLGVRGK peptide and quencher. On the surface of the MSNs, the 5(6)-carboxytetramethylrhodamine hydrochloride (TAMRA) exists in a fluorescence “off state” because of its close proximity to the quencher, 4,4-dimethylamino-azobenzene-4′-carboxylic acid (Dabcyl). However, fluorescence is turned on when the nanoplatform is present in SCC-7 cells because cleavage of the MMP-2 sensitive peptide causes separation of the fluorophore and the quencher. At the same time, the reduced densities of MMP-2 activatable probes on MSNs result in opening of a gate, which induces drug release.[95]

NQO1: NQO1 is a member of NAD(P)H dehydrogenase family that encodes a 2-electron reductase which acts on a variety of xenobiotics and quinones. Given its stress induced upregulation, NQO1 is overexpressed in many cancers.[114] Especially, the level of NQO1 in human liver carcinoma is up to 50-fold higher than that in normal cells.[115] Moreover, it is speculated that upregulation of NQO1 is an early phenomenon occurring in the cell pathological transformation from healthy to cancerous status. Consequently, NQO1 can be used for the cancer early diagnosis and enzyme-triggered drug release.[116]

In 2016, Shin *et al.* described an AIE scaffold for mitochondria targeting and NQO1 enzyme activatable prodrug delivery.[96] This system contains an AIE fluorophore bearing a triphenylphosphonium targeting group and a quinone trigger. After being selectively concentrated in mitochondria of tumor cells, the non-fluorescent AIE scaffold aggregates to form an active AIE dye as a result of NQO1 promoted reduction, cyclization and elimination of quinine. Consequently, a strong fluorescence signal is generated. At the same time, the

AIE aggregates induce disruption of metabolic pathways leading to selective apoptosis of cancer cells.[96] These workers also devised another NQO1 enzyme activated prodrug consisting of the anticancer agent SN-38, a hydroquinone trigger, and a biotin group for targeting folate receptors (Figure 3). The NQO1 activation mechanism of this system is similar to that of the AIE scaffold.[97] In 2015, Liu *et al.* also used a similar strategy to develop a DT-diaphorase activatable CPT prodrug.[98]

PTK7: PTK7, also known as colon carcinoma kinase 4, is a receptor kinase that plays a key role in signal transduction across cell membranes. PTK7 is known to be highly expressed in colon cancer but not in normal colon cells. Hence, this enzyme can be employed as a biomarker for assessing tumor progress.[117,118]

In 2016, Chu's group described a PTK7 activatable theranostic approach involving a "structure-switching aptamer triggered hybridization chain reaction" (HCR).[99] In this system, the hairpin structure of the aptamer probe blocks binding of a signal probe. However, the aptamer undergoes structure switching upon binding to PTK7 in the cancer cells, which results in initiation of HCR with signal probes. Hybridization of signal probes to the aptamer results in an enhanced fluorescent signal caused by separation from the quencher Also hybridization recruits HCR with cisplatin prodrug probes and signal probes, which results in amplification of the fluorescence signal and accumulation of a cisplatin prodrug in cancer cells (Figure 4). Results of *in vitro* studies indicate that this approach enables efficient PTK7 detection with a limit of 1 pM and a high anticancer effect on the PTK7 overexpressed cells.[99]

Caspases: Caspases are a family of cysteine-dependent, aspartate-directed proteases that have attracted increasing attention in the context of apoptosis monitoring because they are crucial mediators and effectors of apoptosis.[119,120] In 2014, Yuan *et al.* developed a Pt(IV) prodrug for targeted therapy and apoptosis monitoring in which one axial position of the metal is occupied by a cRGD targeting group and the other contains a caspase-3 cleavable Asp-Glu-Val-Asp (DEVD) peptide linked AIE fluorophore.[100] This prodrug can be selectively delivered into cancer cells because of the specific affinity of cRGD to $\alpha_v\beta_3$ integrin. After cellular uptake and subsequent reduction of Pt(IV) in the prodrug to produce the active Pt(II) anticancer form, cell apoptosis is induced and activated caspase-3 cleaves the DEVD sequence. As a result, the hydrophobic AIE fluorophore aggregates, which causes enhanced fluorescence emission that can be utilized for real-time monitoring of Pt(II) drug-induced apoptosis.[100]

In 2015, Li *et al.* reported that a human serum albumin (HSA) nanocarrier system can be used for controlled drug delivery and simultaneous evaluation of anticancer efficacy.[101] The system is comprised of a nanocarrier conjugated with a chemotherapeutic agent Pt(IV) prodrug and a caspase-3 responsive fluorescence probe containing a fluorescence donor (Cy5) linked with a quencher (Qsy21) through CGDEVDAK peptide (Figure 5). Upon laser irradiated, an active Pt species is released that causes cellular apoptosis, which subsequently leads to activation of caspase-3. As a result, CGDEVDAK peptide is cleaved and the fluorescence of Cy5 is turned on. Thus, this system enables cancer treatment and real-time imaging.[101]

Wang *et al.* developed a ferritin nanocage for real-time monitoring of PDT-induced apoptosis.[102] In this theranostic agent, zinc(II) phthalocyanine (ZnPc) photosensitizers is embedded in a nano-assembly produced by reassembly of both ferritin nanoparticles (FRT) modified with Cy5.5 NIR dye (FRT-C3) through a caspase-3 specific substrate (GDEVDAPC peptide) and FRT modified with BHQ3 quencher (FRT-BHQ3). The formed nanocage is transferred into cancer cells *via* a FRT-specific transferrin receptor 1 (TfR1). Upon 630 nm laser irradiation, the unquenched ZnPc generates ROSs, which induce apoptosis of cancer cells. Consequently, caspase-3 cleaves the GDEVDAPC peptide that activates Cy5.5 leading to a strong fluorescence signal. The cage has a high potential for use as a novel tool for imaging PDT-induced apoptosis both *in vitro* and *in vivo*.[102] However, the issue of whether the fluorescence of ZnPC affects the output signal of this monitoring system needs to be addressed.

In a more comprehensive study, Zhang's group developed a ratiometric theranostic, comprised of both a fluorophore and photosensitizer, that can be used not only for PDT but also to monitor PDT-induced apoptosis.[103] Specifically, the system contains protoporphyrin IX (PpIX) as photosensitizer, 5(6)-carboxyl-fluorescein (FAM) connected with 4-(dimethlaminoazo)-benzene-4-carboxylic acid (Dabcyl) *via* a linker of caspase-3 responsive DEVD peptide as Förster resonance energy transfer (FRET) fluorophore pair, and RGD as an $\alpha_v\beta_3$ integrin targeting group. After the activation of caspase-3 by the apoptosis effect of PDT, DEVD is cleaved. This process leads to recovery of the fluorescence of FAM. Moreover, fluorescence of PpIX can be used as an internal reference for ratiometric probing of the therapeutic response.[103]

3.1.2. Non-enzymatic Protein-Driven Turn on Theranostics—In addition to enzymatic protein-driven strategies, two examples of non-enzymatic protein-driven turn on theranostics have been described. One is based on a folate receptor response. Folate receptor (FR) is overexpressed in a variety of cancer cells, such as brain, nose, ovary, breast, lung, colon and prostate cancer, but it has a very low expression in some normal cells.[121–123] Thus, FR is broadly used as cancer targeting biomarker. In addition, because of the high binding affinity ($K_d \cong 10^{-10}$ M) of folate to FR, folate-conjugation has been utilized to achieve FR-targeted delivery of a wide range of theranostics.[124]

In 2014, Jin *et al.* described a theranostic system that is based on FR targeting-triggered disruption of a porphysome nanostructure for activabtable FLI and PDT.[104] The folate-porphysome system is constructed by assembly of porphyrin-phospholipid conjugates and 1% of folate-PEG-lipid. The assembled folate-porphysome displays quenching of $^1O_2$ production (over 90%) as well as fluorescence (over 99%) compared to that of the corresponding disassembled form of the nanohybrid. FR facilitates cellular uptake of folate-porphysome into cancer cells and simultaneously induces efficient disruption of the nanohybrid. These events lead to recovery fluorescence emission and $^1O_2$ production by the photosensitizer. The results show that FR-targeted folate-porphysome under a low laser dose (671 nm, 150 mW/cm^2, 100 J/cm^2) completely inhibits tumor growth, an observation which demonstrates the promising applicability of targeting-triggered PDT reactivation of porphysome in cancer-specific therapy.[104]

Another non-enzymatic protein activatable theranostics is based on the transferrin receptor, a transmembrane glycoprotein that plays a vital role in iron transport and cellular respiration.[125] Although TfR is present in normal cells, its upregulated expression at a much higher proliferation rate ubiquitously occurs in abnormal cells. It has been speculated that the expression level of TfR correlates with cancer progression. Therefore, quantitative detection of TfR can be used for early diagnosis of cancer.[126,127] In addition, after binding with transferrin (Tf), the TfR-Tf complex is internalized into clathrin-coated pits *via* endocytosis. This endocytosis process can even facilitate penetration of biologically intrinsic barriers such as the blood-brain barrier (BBB). This property demonstrates the significance of TfR as a delivery target for therapeutic agents.[128]

In 2016, Liu's group described an AIE probe, composed of a conjugate between AIEgen (TPRTH) and a targeting linker (T7), for TfR sensing and activatable PDT.[105] T7 peptide is a better ligand for TfR than transferrin because it utilizes a different higher affinity binding site. This property avoids unnecessary competition caused by endogenous transferrin. The presence of the hydrophilic T7 linker enables this probe to remain in a non-aggregated, nearly non-fluorescent form in aqueous solution. However, in the presence of TfR, fluorescence of the probe is turned on with a TfR detection limit of 0.45 μg/mL. In addition, light irradiation (400–800 nm, 100 mW/cm^2, 5 min) triggers photodynamic ablation of the targeted cancer cells.[105]

In addition to FR and TfR, many other non-enzymatic proteins are overexpressed in either cancer or non-cancer cells in tumor tissues. For example, overexpression of the biotin receptor (BR) is known to be higher than that of FR in a large number of cancer cell lines, including breast (JC, 4T1, MMT06056), ovarian (ID8, Ov2008), colon (Colo-26), lung (M109), mastocytoma (P815), renal (RD0995, RENCA) and leuke (L1210FR) cancers.[129–131] Also, tumor-associated macrophage, a type of non-cancer cells related to a variety of solid tumors including hepatocellular, ovarian, breast, and pancreatic carcinomas, highly expresses scavenger receptor-A (SR-A).[132,133] a_vb_3 integrin and vascular endothelial growth factor receptor (VEGFR) are also promising targetable biomarkers for specific therapeutic agent delivery systems.[134,135] Therefore, many more potential strategies exist to design and construct special activatable theranostics for bioimaging and therapy that operate using non-enzymatic protein stimuli.

3.2. mRNA-Driven Turn on Theranostics

Messenger RNA (mRNA), a subtype of RNA, is a single stranded ribonucleic acid that carries a portion of genetic information in transcription process. Some mRNAs are closely associated with certain stages of various disease and, as a result, can be utilized as reliable biomarkers for cancer diagnosis.[136] Therefore, studies of mRNAs are critical in providing insight into basic biological processes and identifying diagnostic and therapeutic targets. Recently, mRNA-targeted theranostics based on conjugation of molecular beacons (MB) with fluorophores, AuNPs, Q-dots or other interesting materials have been developed as powerful theranostics for mRNA detection and cancer-specific therapy.

In Table 3 are summarized mRNA-driven, turn on theranostics that have been reported in recent years. An interesting approach for both mRNA probing and gene therapy that uses a

distinctive MB system called a MB micelle flare (MBMF) was reported by Chen *et al.* in 2013.[137] MBMFs were constructed by self-assembly of diacyllipid-MB building blocks in aqueous solution (Figure 6). The MB contains a hairpin structure that consists of a mRNA recognition DNA sequence flanked by two complementary sequences, a fluorophore and a quencher. Because the fluorophore is located in close proximity to the quencher in the hairpin structure, its fluorescence is efficiently quenched (off state). Just like a pyrotechnic flare capable of generating brilliant light after being activated, MBMF undergoes a burst of fluorescence emission upon mRNA binding which induces a conformational change. The opening of hairpin structure (ON state) inhibits gene expression by arresting translation, which then induces significant apoptosis of the targeted cancer cells. The authors believe that the MBMF system has many advantageous features including ease of preparation, improved enzymatic stability, promising target selectivity, efficient cellular uptake and superior biocompatibility.[137] This initial study inspired the use of MB strategy to design and construct a variety of mRNA responsive graphene-QD-MB,[138] QD-TMB,[139] polypyrrole-MB,[140] AuNP-MB [141] and UCNPs-MB/DOX systems.[142]

Another example of a mRNA-driven, turn on theranostic was described by Tang's group in 2015. The system is based on an AuNP flare-capped MSN and can be used to detect human mutT homologue MTH1 mRNA and suppress MTH1 activity (Figure 7).[143] The flares are fabricated from AuNPs whose shells are modified with MTH1 mRNA recognition sequences that are hybridized to the Cy5 labelled reporter sequence. After loading the MTH1 inhibitor, S-crizotinib, into the pores of MSN, the flares are immobilized on the surface of MSN via linkage of the Cy5 labelled reporter sequence. Because the flares block the pore of MSN release of S-crizotinib is inhibited and because Cy5 is located in close proximity to AuNP thus the fluorescence is quenched. However, AuNPs are liberated from the MSN when the mRNA recognition sequence hybridizes with MTH1 mRNA in cancer cells to form a more stable duplex. This process leads to opening of the MSN pores along with consequent recovery of fluorescence emission and S-crizotinib release. The results of *in vitro* and *in vivo* studies demonstrate the potential of the AuNP flares-capped MSN system for detection of MTH1 mRNA in living organisms and for effectively killing tumors through inhibition of MTH1 activity.

3.3. ROS-Driven Turn on Theranostics

Reactive oxygen species (ROSs) such as hydrogen peroxide (H_2O_2), hydroxyl radical ($[OH]^{\bullet}$), superoxide ($[O_2]^{\bullet-}$), hypochlorous acid (HOCl), $^1O_2$ and peroxynitrite ($ONOO^-$) are highly reactive chemicals. In biological systems, ROSs are constantly generated and eliminated under oxidative stress and relaxation conditions. As a result, these species are usually present at low balanced levels under normal physiologic conditions at which they play important roles in a wide variety of biological events including cell signaling, homeostasis, proliferation and aging.[144] Cancer cells contain higher levels of ROSs than do normal cells, a partial consequence of oncogenic stimulation, mitochondrial malfunction and increased metabolic activity.[145] These abnormal characteristic have been employed to exploit ROSs as a promising targets for the development of turn on theranostics. Recent examples of ROS-activated theranostics are displayed in Table 4. In organic chemical reactions, H_2O_2 is a neutral nucleophile that serves as an efficient two-electron electrophilic

oxidant. In addition, this ROS is known to react with substances containing a boronate moiety (boronic acid or their esters) to generate products that undergo dissociation to form non-cytotoxic products. Because reactions between H_2O_2 and boronates are chemospecific, biocompatible and bioorthogonal, boronate conjugates have received attention in the context of the development of H_2O_2-activated anticancer prodrugs. For example, Kim *et al.* utilized a boronate ester as a trigger and coumarin as a fluorescence reporter to monitor the H_2O_2-induced release of the anticancer drug SN-38 (Figure 8).[146] In PBS buffer containing 10% DMSO, the new prodrug **7** (5 μM) displays weak fluorescence around 453 nm. The intensity of this emission increases by about 8.3-fold when **7** is treated with 300 μM H_2O_2. The results of kinetics studies indicate that the active drug SN-38 is released from the conjugate in less than 10 min. In addition, the finding shows that the prodrug is selectively activated by H_2O_2 over other tested ROSs. Cell experiments demonstrate that the prodrug is a promising marker for H_2O_2 in lysosomes. More importantly, the therapeutic efficacy of **7** was probed using a metastatic lung tumor model developed by B16F10 melanoma cells through intravenous injection. After intratracheal treatment with the prodrug (dose per time: 0.25 mg/kg; four times treatment), tumor growth in lung tissues is significantly reduced and the survival time of mice is prolonged compared with the control group.[146] Other H_2O_2-activated theranostics based on the same responsive unit such as the phenylboronic ester-quinone cyanine-7 (QCy7)-CPT prodrug system[147] and arylboronate ester-capped polymersomes nanosystem have been developed.[148] All of these conjugates possess promising H_2O_2 activatable features.

Other H_2O_2 responsive materials such as MnO_2 nanosheets[149] and Fe^{3+}-doped C_3N_4 nanofusiform[150] have been explored as part of the development of new theranostics. The MnO_2 nanosheets-based theranostic system (Figure 9) takes advantage of the fact that acidic H_2O_2 reduces MnO_2 to form Mn^{2+} along with oxygen. Based on this information, upconversion nanoprobes ($NaYF_4$:Yb/Er/Tm nanosphere coated with a photosensitizer-incorporated dense silica shell) loaded MnO_2 nanosheets (UCSMs) were constructed for pH-/ H_2O_2-responsive upconversion luminescent imaging (UCLI) and oxygen-enhanced synergetic RT/PDT. In the absence of H_2O_2, emission from the upconversion nanoprobe is quenched by the MnO_2 nanosheets. However, H_2O_2-induced reduction of MnO_2 under acidic conditions liberates upconversion nanoparticles from the nanosheets, which leads to UCL. As a result, the overall process can be employed to diagnose or monitor acidic tumor microenvironment and the overproduction of H_2O_2 in solid tumor tissues. In addition, the large amount of oxygen produced *in situ* by the H_2O_2-MnO_2 redox reaction significantly improves the therapeutic effects of RT/PDT promoted X-ray/NIR irradiation. It is noteworthy that intelligent 2D nanomaterials have also been used to construct theranostic agents for oxygen-elevated therapy.[149]

3.4. Glutathione-Driven Turn on Theranostics

The tripeptide glutathione (GSH) participates as a cellular protection agent by controlling a variety of cellular processes including cell differentiation, metabolism, antioxidant defense and balancing carcinogenicity.[155] Moreover, GSH plays a critical role in maintaining detoxification and antioxidation equilibria of many cellular functions through which neutralization of ROSs in conjunction with its conversion from a reduced to oxidized form

(glutathione disulfide, GSSG). GSSG is readily reduced by the enzyme GSH reductase. However, GSH deficiency or overexpression causes dysfunction of related cellular processes, which results in a high level of oxidative stress. This is particularly true in cancer cells where the production and expression levels of GSH are typically higher (about 10 mM in many cancer cells) than those in normal cells.[156] Therefore, a number of approaches for the development of cancer targeted therapeutic agent release and activation are based on reaction of GSH.

To date, a variety of theranostics that rely on GSH-responsive strategies have been described (Table 5). As shown in Table 5, most of the GSH-driven turn on theranostics that exploit disulfide-based processes contain a fluorophore, a chemotherapeutic drug and a tumor targeting group (Figure 10). These theranostic systems operate by cleavage of disulfide bonds and subsequent release of an activated drug and generation of an enhanced fluorescence signal. In principle, systems of this type not only enable more specific and precise monitoring of drug dosage levels, but they also provide information about the diversified cellular uptake, release and activation mechanisms that are associated with chemotherapeutic drug delivery and design.[157]

In addition to disulfides, another widely used GSH-responsive organic moiety is the sulfonyl group. For instance, a 2,4-dinitrobenzenesulfonyl substituted phthalocyanine developed by He *et al.* in 2015 has an excellent GSH-responsive photoactivity that can be used advantageously for cancer targeted imaging and PDT.[163] In this system (Figure 11), reactions of 2-hydroxy-phthalocyaninatozinc(II) (**1**) with 2,4-dinitrobenzenesulfonyl chloride generates the target **2** in a reasonably high yield (70%). Owing to the strong electron-withdrawing effects of 2,4-dinitrobenzenesulfonyl group, fluorescence emission and $^1O_2$ generation of **2** are effectively quenched while the ground-state properties of the phthalocyanine core remain nearly unchanged. However, in the presence of GSH (about 1 mM), the sulfonyl ester in **2** is cleaved, which leads to a gradual increase of the fluorescence intensity during the first 2 h and significantly enhanced $^1O_2$ production. Glutathione monoester (GSH-OEt), which can be readily internalized by cancer cells and quickly hydrolyzed to form GSH, was used along with **2** to explore the effect of GSH concentrations at cellular level. Compared to those of 2-hydroxy-phthalocyaninatozinc(II) (**1**), the photoactivity efficiencies of **2** including both fluorescence and singlet oxygen production are improved by GSH-OEt in cancer cells. In addition, **2** exhibits a significant killing effect on MCF7 cells with an IC_{50} value of 0.19 μM, which is similar to that of **1** (0.13 μM). More importantly, the results of *in vivo* studies show that the fluorescence from mice bearing HT29 tumor gradually increases over time after treatment with **2**, whereas mice injected with **1** remain in an “always-on” state.[163] These results suggest the importance of the turn-on strategy for diagnosing diseases.

Fan *et al.* recently described an inorganic material-based GSH-responsive system that was devised using a design that is different from an organic groups-based strategy.[168] In this system, photosensitizer Ce6 is employed as a fluorescence reporter as well as a therapeutic agent. Owing to their ability to adsorb organic molecules and their broad absorption spectrum (about 200–600 nm), MnO_2 nanosheets are used as a carrier as well as a quencher in this system. MnO_2 nanosheets in this system are reduced by GSH, which causes

subsequent release Ce6 with recovered photoactivities for FLI and PDT. In addition to their function to protect photosensitizers from self-destruction and their ability to facilitate cellular uptake, MnO_2 nanosheets decrease the level of GSH level in targeted cells, which in turn efficiently enhances the toxic effect of $^1O_2$ produced by photosensitizer. Thus, this photosensitizer-MnO_2 nanosystem incorporates a method to solve the traditional problem of PDT that is an unsatisfactory therapeutic efficacy caused by inefficient delivery of photosensitizers and the antioxidant effects of GSH. In addition, the results of *in vivo* experiments show that the fluorescence intensity of photosensitizer-MnO_2 treated tumors increase in the first hour whereas that of free photosensitizer decreases gradually after administration. These results highlight the promising potential of photosensitizer-MnO_2 nanosystems in GSH-activatable imaging. However, because *in vivo* experiments were conducted by using intratumoral injection, more detailed information is needed about the bio-distribution following intravenous injection.

3.5. Hypoxia-Driven Turn on Theranostics

Tumor microenvironments are very different from those of healthy tissues. One distinguished feature is the low partial pressure of oxygen in cancer cells known as hypoxia. The oxygen concentration in many solid tumors is about 4% and sometimes it is non-measurable in local tumor environments.[174] This phenomenon is caused by the consumption of oxygen within about 100 μm of the inadequate tumor vasculatures by quickly proliferating cancer cells. This event prevents oxygen from diffusing into large regions of tumor tissues. In order to allow uninterrupted growth and proliferation in a hypoxic environment of this type, cancer cells rapidly adapt by using their genetic instability.[175,176] In addition, hypoxia is known to be associated with extracellular matrix remodeling, resistance to some therapeutic modalities (such as CHT and RT), poor prognosis and increased metastasis.[177] Real-time quantitative monitoring of oxygen concentrations in living organisms not only enables accurate cancer diagnosis, but it also can be utilized for evaluating the prognosis of therapeutic effects. Therefore, numerous efforts have focused on the development of hypoxia-triggered activation of theranostics. Some recent examples are summarized in Table 6.

Thus far, three representative hypoxia-responsive moieties, including nitrobenzyl alcohols, nitroimidazoles and azo linkers (Figure 12), have been utilized to design fluorescence probes, prodrugs and nanocarriers.[184] Generally, the hypoxia-responsive moieties contain reducible functionality such as nitro, quinone and azo groups, which are reduced when present in hypoxic environments. Because the reduction of these hypoxia-responsive moieties generates hydrophilic groups, the physical and chemical properties of the responsive systems, including hydrophilicity and size distribution, can dramatically change in response to hypoxia. Very recently, Kumar *et al.* reported the nitrobenzyl alcohol-based hypoxia activatable anticancer theranostic agent **4**, which consists of a biotin group, a drug SN38 and a nitro unit.[179] SN38 is a toposisomerase I inhibitor that is used for cancer therapy and its inherent fluorescence permits its use as a fluorophore for diagnosis. The biotin group is incorporated as a tumor-targeting moiety. Moreover, the nitro unit in this system is activated specifically in hypoxic environments, whereas it remains inactive under other conditions. The theranostic agent **4** is selectively activated in tumor spheroids and solid

tumor tissues, upon which it releases SN38 and accompanied by enhanced fluorescent emission. The results of *in vitro* and *in vivo* experiments show that **4** selectively inhibits the activity of cancer cells and the growth of solid tumors. A hypoxia-activated anticancer prodrug based on a gemcitabine-cinnamic ester-nitrobenzyl platform[178] and a polymer-drug delivery system was also reported.[181]

A nitroimidazole-based hypoxia activatable phototrigger system was described by Zhu's group.[182] In their study, etoposide, chosen as the topoisomerase inhibitor, is caged by 7-aminocoumarin phototrigger. The phototrigger is locked by a hypoxic responsive nitroimidazole that serves as an electron acceptor quencher to prevent photocleavage of the coumarin moiety. Under hypoxic conditions and light irradiation, the anticancer drug is released from the conjugate and the fluorescence intensity is significantly increased owing to the photo-SN1 cleavage mechanism. Similarly, a hypoxia-responsive photoactivable nanocarrier system comprised of polymer capable of NIR imaging and PDT and a nitroimidazole moiety was also found to have promising imaging capabilities and anticancer effects *in vivo* (Figure 13).[183]

3.6. Slight Acid-Driven Turn on Theranostics

Another distinguishing feature of tumor microenvironments is their slightly acid nature. Specifically, the extracellular pH in tumor tissues is usually lower (6.5 to 6.9) than in normal tissues, whereas cancer cells have a neutral pH (7.2 to 7.4).[185] This phenomenon is a result of the increased glycolysis and proton-pump activities on plasma membranes of cancer cells, which cause more abundant production of lactic acid that easily leaches into extracellular milieu.[186,187] Thus, the utilization of theranostics that efficiently generate visual signals and enhance therapeutic activities under slightly acidic conditions but are less active under neutral conditions, would be useful for cancer-specific imaging and therapy. As summarized in Table 7, a number of slight acid-activatable theranostics have been developed recently. These strategies for the most part are based on the protonation of amine groups, and acid cleavage of hydrazone linkers or acid sensitive inorganic materials.

3.6.1. Based on Protonation of Amine Group—By taking advantage of structural transformations induced by protonation of amine groups, Tian *et al.* devised an acid (pH 5.0) responsive selenium rubyrin-loaded nanoparticle for use as an activatable photosensitizer for FLI and PDT.[189] Selenium in the rubyrin ($NMe_2Se_4N_2$) core increases its ability to produce $^1O_2$ owing to a heavy atom effect on intersystem crossing from the rubyrin singlet to triplet excited state (Figure 14). Dimethlaminophenyl groups at *meso*-positions of rubyrin efficiently quench its excited-state by photoinduced electron transfer, which turns off the generation of $^1O_2$ under neutral conditions. However, photoactivities of the amine-substituted rubyrin are turned on when the tertiary amine groups are protonated under acidic conditions. Under 635 nm light irradiation, protonated $NMe_2Se_4N_2$ has a high photosensitization ability with a $^1O_2$ quantum yield (Φ_Δ) of 0.69 at pH 5.0 compared to 0.06 at pH 7.4. In addition, the FA functionalized nanoparticle facilitates selective delivery to cancer cells through receptor-mediated endocytosis. In a similar manner, Lee *et al.* employed a BODIPY group that is activated under slightly acid condition to construct biosynthetic polypeptide-based nanoparticles. The nanoparticles possess the ability to display pH-

induced turn-on fluorescence, delivery of anticancer drugs and enhancement of receptor-mediated endocytosis.[194] In 2015, Tian *et al.* also developed a diethylaminophenyl substituted BODIPY-based pH-activatable theranostic nanosystem.[201] Owing to the advantage of NIR excitation and emission beyond 800 nm, this theranostic serves as a new paradigm for sensitive fluorescent bioimaging and cancer-targeted PDT.

In 2016, Wang *et al.* reported a weakly acid condition (pH ≤ 6.2) responsive multifunctional nanosized micelle.[218] Collectively, this study presents an excellent example for multimodal imaging (FLI, MRI, and PAI) and combinational therapy (PDT, PTT, and CHT). In this theranostic system, the micelles are composed of pH-responsive diblock copolymer (PDPA), gadolinium-coordinated photosensitizer Ce6, and a pluronic prodrug DOX. Interestingly, this micelle showed silenced photoactivities during blood circulation owing to the FRET effect between Ce6 molecules and PET effect from nitrogen atom of PDPA to Ce6. However, under the trigger of slight acid in endocytic vesicles of cancer cells, its fluorescence emission and ROS generation are dramatically increased, which then caused the cytosol release of DOX. Additionally, this micelle could induce efficient heating effect for enhancing tumor penetration of DOX, tumor specific PTT and PAI. Moreover, in the acidic microenvironment, the dissociation of micelles and access of water molecules to the gadolinium ions permitted an amplified magnetic resonance signal. Comparing to the common theranostic agent that only permits a single imaging modality and a single therapy modality, this robust nanoplatform adequately display the advantages of multimodal imaging guided multimodal therapy in the cancer treatment.

It is worth mentioning that pH-activatable theranostics described above respond to acidic environments that have pH values of about 5.0. This is not an appropriate property for use in the only slightly acidic microenvironments found in tumor tissues, but rather for theranostic applications to condition present in subcellular compartments such as endosome and lysosome. Because normal cells also have acidic subcellular compartments that are similar to those of cancer cells, the pH-activatable theranostics described above are not tumor microenvironment activatable, which limits their cancer specific activation to some extent. To overcome this limitation, Park *et al.* developed an interesting polysaccharide/drug conjugate for tumor-pH (pH 6.8) activatable PDT.[188] In this system, a glycol chitosan backbone with 3-diethylaminopropyl isothiocyanate block is conjugated with Ce6 and PEG block. The conjugate assembles to form a 3-dimensional supramolecular structure at neutral pH, which exists in a Ce6 self-quenched state. However, the supramolecular structure is transformed into an extended random molecule as a result of the change in surface charge occurring under slightly acidic conditions (pH 6.8). In addition, the fact that the pK_b value of 3-diethylaminopropyl isothiocyanate modified glycol chitosan is near 6.8 enables reactivation of fluorescent emission and $^1O_2$ generation caused by protonation of the amine groups. The results show that thus system has a higher efficiency for $^1O_2$ generation at pH 6.8 than at pH 7.4 and that it displays a significantly enhanced anticancer effect against HeLa cells under acidic condition and light irradiation. One of the interesting findings is that the fluorescence signal at the tumor site after *i.v.* injection of this conjugate fluctuates, a phenomenon that is ascribed to the combined operation of pH-induced enhanced fluorescence and clearance or diffusion of the fluorophore.

3.6.2. Based on Acid Cleavable Hydrazone Linker—A hydrazone linker with the structure -C=N-NH-, is typically formed by reaction of hydrazine with an aldehyde or ketone. The hydrazone bond is stable under neutral conditions but is quickly cleaved by aqueous acids. Using hydrazone as a linker, Zhang *et al.* developed an acid responsive nanosystem for combined CHT and PTT (Figure 15).[209] In this system, DOX is conjugated to a FA modified amphiphilic block copolymer *via* a hydrazone linker. In aqueous solution, this conjugate self-assembles to form stable and monodispersed nanoparticles containing IR825. DOX is released rapidly when the conjugate is present in acidic environment (pH < 6.0) owing to the cleavage of hydrazone linker. In addition, encapsulated IR825 efficiently converts NIR light energy to heat, which enables the nanoparticle to serve as a photothermal agent for PTT. The results of *in vitro* studies show that upon light irradiation this nanosystem significantly inhibits the activity of both DOX-sensitive cells (Hela) and DOX-resistant cells (A2780/DOX). At the same time, the enhanced fluorescence of this nanosystem in cancer cells can be used for *in situ* monitoring of drug release. More importantly, an obvious tumor regression was observed in a zebrafish liver hyperplasia model after treatment with this nanoparticle formula.

In 2014, Lau *et al.* described a dual acid and GSH responsive photosensitizer for FLI and cancer-targeted PDT. This theranostic system is composed of conjugate of an asymmetrical silicon (IV) phthalocyanine and ferrocene joined *via* a hydrazone linker and a disulfide bond.[213] More recently, a hydrazone linked zwitterionic phosphorylcholine-AIEgen conjugate was developed for selective drug delivery and pH-responsive drug release, and AIE active FLI.[212]

3.6.3. Based on Acid Sensitive Inorganic Materials—Thus far, several inorganic materials, including calcium carbonate ($CaCO_3$), MnO_2 nanosheet, Fe^{3+}-gallic acid and layered double hydroxides (LDHs), have been used as acid sensitive units in activatable theranostics. For example, polyethylene glycol modified $CaCO_3$ nanoparticles were used by Dong *et al.* as a carrier of Ce6(Mn) and DOX for real-time MRI and cancer-targeted therapy.[210] Because the $CaCO_3$ nanoplatform is stable at pH 7.4 but rapidly degrades at pH 6.5, Ce6(Mn) and DOX can be selectively released in pH-dependent manner. The released Mn^{2+} causes increases in the T_1 signal used for MRI, which enables real-time monitoring of DOX release. According to the results of *in vivo* MRI and FLI studies, this highly pH sensitive nanosystem gradually accumulates in tumor tissues after *i.v.* injection, which accounts for its excellent anticancer activity in combined PDT and CHT.

LDHs, also called anionic nanoclays, are an interesting class of layered inorganic materials that are usually described by the general formula $[M^{2+}_{1-x}M^{3+}_{x}(OH)_2](A^{n-})_{x/n}{\cdot}mH_2O$, where M^{2+}, M^{3+} and A^{n-} correspond to a divalent metal cation, a trivalent metal cation, and a charge-balancing interlayer anion, respectively.[220] In recent years, LDHs have gained considerable interest as drug or gene carriers as a result of their advantageous features including simple preparation, anion exchange properties, good biocompatibility and acid sensitivity.[221,222] Based on this knowledge, Huang and coworkers designed and constructed a tumor-pH responsive nanohybrid (LDH-$ZnPcPS_4$), in which a cationic LDH and a negative phthalocyanine $ZnPcPS_4$ are held together *via* electrostatic interactions (Figure 16).[216] Bare $ZnPcPS_4$ has high photoactivites when irradiated at around 692 nm at

pH 7.4. However, its fluorescence emission and $^1O_2$ production ability are effectively quenched by about 80% when it is loaded onto LDH. Although LDH-$ZnPcPS_4$ has high stability under neutral conditions (pH 7.4), the complex effectively releases $ZnPcPS_4$ under slightly acidic conditions (pH 6.5). This process leads to about 60% regeneration of the photoactivities of $ZnPcPS_4$. The results of *in vitro* studies indicate that LDH-$ZnPcPS_4$ has significant anticancer effects in HepG2 cells (IC_{50} = 0.053 mM) under light irradiation as compared to that of bare $ZnPcPS_4$ (IC_{50} = 1.27 mM). The strategy used to design this theranostic system can be utilized to develop novel photosensitizers that have tumor targeting abilities, slightly acid activatable fluorescence emission and phototoxic effects, and minimal side effects.

4. Conclusion and Outlook

Many dozens of cancer-associated, stimuli-driven, turn-on theranostics have been developed thus far, most of which have been described in the past 5-year period. These theranostic systems are both specific and effective because of differences that exist between tumor tissues and normal tissues with respect to enzyme, non-enzymatic protein and GSH expression, mRNAs, ROS stress levels and microenvironment acidities. The intrinsic fluorescence, ultrasonic wave, magnetic field or other visualizing signals that arise following activation of the theranostics not only enables their use in cancer diagnostic applications but also for *in vivo* imaging guided cancer therapy.

Many activation strategies based on anomalies of cancer cells have been exploited in designing these theranostic systems. However, we believe that in the coming years many conceptually new approaches to the design of cancer-associated, stimuli-driven, turn-on theranostics will be devised. We predict that new and interesting theranostics that employ novel activation mechanisms based on for example newly discovered over-expressed proteins or specific metal ions will be developed during this period. Because most of the existing slight acid-driven turn on theranostics are responsive to acidic conditions with pH values lower than 6.5, which do not match the pH region of tumor microenvironments (pH 6.5 to 6.9), more attention will focus on tumor-pH driven turn-on theranostics.

Most of existing nanotheranostics are based on EPR effect, however, little effort has been made on developing methods or technologies capable of providing information about the tumor microenvironment.[223] Therefore, we expect that stimuli-responsive turn on theranostics will be able to provide an effective approach to measure tumor EPR effect, which will advance the realization of theranostics as well as nanomedicines.

It is also worth mentioning that most theranostic systems are still early in development, and their safety in humans have not been studied. Clearance of these potential theranostic systems from the human body need to be studied. To increase the possibility of clinical translation of theranostics, several points should be taken into account: first, combination of different imaging modalities, such as MRI/PET, FLI/MRI, or PET/CT, will be necessary. As aforementioned, every single imaging modality has its pros and cons. Different imaging modalities are possible to compensate each other. However, the different doses of each imaging agent should be carefully considered because of their different sensitivity. Similarly,

combination of different therapy modalities is also expected. Second, more facile and efficient theranostics, which contain fewer components or even only a single component but still possess multiple functions, should be pursued for clinical translation. Existing multifunctional theranostics, which are capable of activatable multimodal imaging and/or multimodal therapy, usually consist of several components. This “all-in-one” approach suffers from some shortcomings associated with multistep construction and potentially complex toxicity. Finally, biocompatibility should be considered in choosing materials for theranostic design and development. Thus, biodegradable organic materials and natural biological materials will likely be more attractive than non-degradable inorganic materials.

As the limiting factors governing traditional cancer treatments are becoming better understood and addressed, we can expect that the clinical utility of multimodal imaging guided therapy for personalized medicine will grow. It is obvious from inspection of the materials presented in this review that the cancer-associated, stimuli-driven, turn on theranostics strategy will continue to contribute significantly to the field of cancer research.

Acknowledgments

Xiaoyuan Chen is funded by the Intramural Research Program (IRP), National Institute of Biomedical Imaging and Bioengineering (NIBIB), National Institutes of Health (NIH). Juyoung Yoon is funded by a grant from the National Creative Research Initiative programs of the National Research Foundation of Korea (NRF) funded by the Korean government (MSIP) (No. 2012R1A3A2048814). Xingshu Li and Jihoon Kim contributed equally to this work.

Biographies

Dr. Xingshu Li was born in Fujian, China. He received his Ph.D. in biochemical engineering in 2015 from Fuzhou University under the supervision of Prof. Jiandong Huang. Then he joined Prof. Juyoung Yoon’s group as a postdoctoral researcher. His current interests include the design and development of activatable photosensitizers, nanoprobes, and multifunctional theranostic agents.

Dr. Jihoon Kim received his Ph. D. from the Department of Chemistry of POSTECH under the supervision of Prof. Won Jong Kim in 2014. After his postdoctoral experience at

Institutes of Basic Science (IBS), he is currently a postdoctoral researcher at National Institutes of Health (NIH) under the supervision of Dr. Xiaoyuan Chen and focuses on developing various systems for the delivery of nitric oxide/gene/drug.

Prof. Juyoung Yoon received his Ph.D. (1994) from The Ohio State University. After completing postdoctoral research at UCLA and at Scripps Research Institute, he joined the faculty at Silla University in 1998. In 2002, he moved to Ewha Womans University, where he is currently a Distinguished Professor of Department of Chemistry and Nano Science. His research interests include investigations of fluorescent chemosensors, molecular recognition and organic functional materials. Prof. Yoon has published over 260 SCI papers.

Dr. Xiaoyuan (Shawn) Chen is a Senior Investigator and Chief of the Laboratory of Molecular Imaging and Nanomedicine (LOMIN) at the National Institute of Biomedical Imaging and Bioengineering (NIBIB), NIH. Dr. Chen has published over 500 peer-reviewed papers (H-index > 100, total citations > 50,000 based on Google Scholar) and numerous books and book chapters. He was elected to the AIMBE's College of Fellows (2017), received the ACS Bioconjugate Chemistry Lecturer Award (2016), NIH Director's Award (2014) and NIBIB Mentor Award (2012). He is the founding editor of journal "Theranostics" (2015 IF = 8.854).

References

1. Ferlay J, Soerjomataram I, Dikshit R, Eser S, Mathers C, Rebelo M, Parkin DM, Forman D, Bray F. Int J Cancer. 2015; 136:E359. [PubMed: 25220842]
2. Siegel RL, Miller KD, Jemal A. CA Cancer J Clin. 2016; 66:7. [PubMed: 26742998]
3. Ryu JH, Lee S, Son S, Kim SH, Leary JF, Choi K, Kwon IC. J Control Release. 2014; 190:477. [PubMed: 24780269]
4. Kojima R, Aubel D, Fussenegger M. Cur Opin Chem Bio. 2015; 28:29.
5. Kumar R, Shin WS, Sunwoo K, Kim WY, Koo S, Bhuniya S, Kim JS. Chem Soc Rev. 2015; 44:6670. [PubMed: 26118960]
6. Wang Z, Niu G, Chen X. Pharm Res. 2014; 31:1358. [PubMed: 23765400]
7. Xie J, Lee S, Chen X. Adv Drug Deliv Rev. 2010; 62:1064. [PubMed: 20691229]
8. Mura S, Couvreur P. Adv Drug Deliv Rev. 2012; 64:1394. [PubMed: 22728642]

9. Kim TH, Lee S, Chen X. Expert Rev Mol Diagn. 2013; 13:257. [PubMed: 23570404]
10. Bertrand N, Wub J, Xu X, Kamaly N, Farokhzad OC. Adv Drug Deliv Rev. 2014; 66:2. [PubMed: 24270007]
11. Park J, Singha K, Son S, Kim J, Namgung R, Yun CO, Kim WJ. Cancer Gene Ther. 2012; 19:741. [PubMed: 23018622]
12. Chari RVJ, Miller ML, Widdison WC. Angew Chem Int Ed. 2014; 53:3796.
13. Warram JM, de Boer E, Sorace AG, Chung TK, Kim H, Pleijhuis RG, van Dam GM, Rosenthal EL. Cancer Metastasis Rev. 2014; 33:809. [PubMed: 24913898]
14. Ornes S. Proc Natl Acad Sci USA. 2013; 110:13695. [PubMed: 23964113]
15. Maeda H. Adv Drug Deliv Rev. 2015; 91:3. [PubMed: 25579058]
16. Li SD, Huang L. Biochim Biophys Acta. 2009; 1788:2259. [PubMed: 19595666]
17. Blanco E, Shen H, Ferrari M. Nat Biotechnol. 2015; 33:941. [PubMed: 26348965]
18. Kim YH, Min KH, Wang Z, Kim J, Jacobson O, Huang P, Zhu G, Liu Y, Niu G, Chen X. Nanoscale in revision.
19. Wu L, Qu X. Chem Soc Rev. 2015; 44:2963. [PubMed: 25739971]
20. Caldorera-Moore ME, Liechty WB, Peppas NA. Acc Chem Res. 2011; 44:1061. [PubMed: 21932809]
21. Lee MH, Kim HJ, Yoon S, Park N, Kim JS. Org Lett. 2008; 10:213. [PubMed: 18078343]
22. Tang Y, Yang HR, Sun HB, Liu SJ, Wang JX, Zhao Q, Liu XM, Xu WJ, Li SB, Huang W. Chem Eur J. 2013; 19:1311. [PubMed: 23255155]
23. Lee DE, Koo H, Sun IC, Ryu JH, Kim K, Kwon IC. Chem Soc Rev. 2012; 41:2656. [PubMed: 22189429]
24. de Jong M, Essers J, van Weerden WM. Nat Rev Cancer. 2014; 14:481. [PubMed: 24943811]
25. Nie L, Chen X. Chem Soc Rev. 2014; 43:7132. [PubMed: 24967718]
26. Rao J, Dragulescu-Andrasi A, Yao H. Curr Opin Biotech. 2007; 18:17. [PubMed: 17234399]
27. Yi X, Wang F, Qin W, Yang X, Yuan J. Int J Nanomed. 2014; 9:1347.
28. Frangioni JV. Curr Opin Chem Biol. 2003; 7:626. [PubMed: 14580568]
29. Pinaud F, Michalet X, Bentolila LA, Tsay JM, Doose S, Li JJ, Iyer G, Weiss S. Biomaterials. 2006; 27:1679. [PubMed: 16318871]
30. Chen G, Qiu H, Prasad PN, Chen X. Chem Rev. 2014; 114:5161. [PubMed: 24605868]
31. He X, Wang K, Cheng Z. Wiley Interdiscip Rev Nanomed Nanobiotechnol. 2010; 2:349. [PubMed: 20564463]
32. Qin S, Caskey CF, Ferrara KW. Phys Med Biol. 2009; 54:R27. [PubMed: 19229096]
33. Son S, Min HS, You DG, Kim BS, Kwon IC. Nano Today. 2014; 9:525.
34. Lindner JR. Nat Rev Drug Discovery. 2004; 3:527. [PubMed: 15173842]
35. Willmann JK, Paulmurugan R, Chen K, Gheysens O, Rodriguez-Porcel M, Lutz AM, Chen IY, Chen X, Gambhir SS. Radiology. 2008; 246:508. [PubMed: 18180339]
36. Nakatsuka MA, Mattrey RF, Esener SC, Cha JN, Goodwin AP. Adv Mater. 2012; 24:6010. [PubMed: 22941789]
37. Min HS, Kang E, Koo H, Lee J, Kim K, Park RW, Kim IS, Choi Y, Kwon IC, Han M. Biomaterials. 2012; 33:936. [PubMed: 22050793]
38. Min HS, Son S, Lee TW, Koo H, Yoon HY, Na JH, Choi Y, Park JH, Lee J, Han MH, Park R-W, Kim IS, Jeong SY, Rhee K, Kim SH, Kwon IC, Kim K. Adv Funct Mater. 2013; 23:5518.
39. Min KH, Min HS, Lee HJ, Park DJ, Yhee JY, Kim K, Kwon IC, Jeong SY, Silvestre OF, Chen X, Hwang YS, Kim EC, Lee SC. ACS Nano. 2015; 9:134. [PubMed: 25559896]
40. Hoult DI, Lauterbur PC. J Magn Reson. 1979; 34:425.
41. Terreno E, Castelli DD, Viale A, Aime S. Chem Rev. 2010; 110:3019. [PubMed: 20415475]
42. Britton MM. Chem Soc Rev. 2010; 39:4036. [PubMed: 20508883]
43. Xie J, Liu G, Eden HS, Ai H, Chen X. Acc Chem Res. 2011; 44:883. [PubMed: 21548618]
44. Liu G, Gao J, Ai H, Chen X. Small. 2013; 9:1533. [PubMed: 23019129]
45. Terreno E, Aime S. Front Pharmacol. 2015; 6:290. [PubMed: 26696890]

46. Wang YXJ. Quant Imaging Med Surg. 2011; 1:35. [PubMed: 23256052]
47. Xiao YD, Paudel R, Liu J, Ma C, Zhang ZS, Zhou SK. Int J Mol Med. 2016; 38:1319. [PubMed: 27666161]
48. Weinmann HJ, Ebert W, Misselwitz B, Schmitt-Willich H. Eur J Radiol. 2003; 46:33. [PubMed: 12648800]
49. Lusic H, Grinstaff MW. Chem Rev. 2013; 113:1641. [PubMed: 23210836]
50. Shilo M, Reuveni T, Motiei M, Popovtzer R. Nanomedicine. 2012; 7:257. [PubMed: 22339135]
51. Lee N, Choi SH, Hyeon T. Adv Mater. 2013; 25:2641. [PubMed: 23553799]
52. Brenner DJ, Hall EJ. N Engl J Med. 2007; 357:2277. [PubMed: 18046031]
53. Christiansen C. Toxicology. 2005; 209:185. [PubMed: 15767033]
54. Pimlott SL, Sutherland A. Chem Soc Rev. 2011; 40:149. [PubMed: 20818455]
55. Ramos de Carvalho JE, Verbraak FD, Aalders MC, van Noorden CJ, Schlingemann RO. Surv Ophthalmol. 2014; 59:393. [PubMed: 24529711]
56. Meikle SR, Beekman FJ, Rose SE. Drug Discov Today. 2006; 3:187.
57. Kim C, Favazza C, Wang LV. Chem Rev. 2010; 110:2756. [PubMed: 20210338]
58. Xu M, Wang LV. Rev Sci Instum. 2006; 77:041101.
59. Wang LV, Hu S. Science. 2012; 335:1458. [PubMed: 22442475]
60. Wang S, Huang P, Chen X. Adv Mater. 2016; 28:7340. [PubMed: 27255214]
61. Alouane A, Labruere R, Le Saux T, Schmidt F, Jullien L. Angew Chem Int Ed. 2015; 54:7492.
62. Gordon MR, Canakci M, Li L, Zhuang J, Osborne B, Thayumanavan S. Bioconjug Chem. 2015; 26:2198. [PubMed: 26308881]
63. Choi KY, Swierczewska M, Lee S, Chen X. Theranostics. 2012; 2:156. [PubMed: 22400063]
64. Mura S, Nicolas J, Couvreur P. Nat Mater. 2013; 12:991. [PubMed: 24150417]
65. Torchilin VP. Nat Rev Drug Discov. 2014; 13:813. [PubMed: 25287120]
66. Saravanakumar G, Kim J, Kim WJ. Adv Sci. 2016; doi: 10.1002/advs.201600124
67. Kim J, Kim J, Jeong C, Kim WJ. Adv Drug Deliver Rev. 2016; 98:99.
68. Davidson BL, Breakefield XO. Nat Rev Neurosci. 2003; 4:353. [PubMed: 12728263]
69. Park TG, Jeong JH, Kim SW. Adv Drug Deliver Rev. 2006; 58:467.
70. Liu G, Choi KY, Bhirde A, Swierczewska M, Yin J, Lee SW, Park JH, Hong JI, Xie J, Niu G, Kiesewetter DO, Lee S, Chen X. Angew Chem Int Ed. 2012; 51:445.
71. Liu G, Swierczewska M, Lee S, Chen X. Nano Today. 2010; 5:524. [PubMed: 22473061]
72. Shim MS, Kwon YJ. Adv Drug Deliver Rev. 2012; 64:1046.
73. Terasawa T, Dvorak T, Ip S, Raman G, Lau J, Trikalinos TA. Ann Intern Med. 2009; 151:556. [PubMed: 19755348]
74. Olsen DR, Bruland OS, Frykholm G, Norderhaug IN. Radiother Oncol. 2007; 83:123. [PubMed: 17499374]
75. Langley SEM, Laing R. BJU Int. 2002; 89:241. [PubMed: 11856104]
76. Volkert WA, Hoffman TJ. Chem Rev. 1999; 99:2269. [PubMed: 11749482]
77. Mroz P, Szokalsk A, Wu MX, Hamblin MR. PLoS One. 2010; 5:e15194. [PubMed: 21179470]
78. Celli JP, Spring BQ, Rizvi I, Evans CL, Samkoe KS, Verma S, Pogue BW, Hasan T. Chem Rev. 2010; 110:2795. [PubMed: 20353192]
79. Juarranz A, Jaen P, Sanz-Rodriguez F, Cuevas J, Gonzalez S. Clin Transl Oncol. 2008; 10:148. [PubMed: 18321817]
80. Hopper C. Lancet Oncol. 2000; 1:212. [PubMed: 11905638]
81. Bechet D, Couleaud P, Frochot C, Viriot ML, Guillemin F, Barberi-Heyob M. Trends Biotechnol. 2008; 26:612. [PubMed: 18804298]
82. Lal S, Clare SE, Halas NJ. Acc Chem Res. 2008; 41:1842. [PubMed: 19053240]
83. Melancon MP, Zhou M, Li C. Acc Chem Res. 2011; 44:947. [PubMed: 21848277]
84. Zhou F, Xing D, Ou Z, Wu B. J Biomed Opt. 2009; 14:021009. [PubMed: 19405722]

85. Sun Z, Xie H, Tang S, Yu XF, Guo Z, Shao J, Zhang H, Huang H, Wang H, Chu PK. Angew Chem. 2015; 127:11688.
86. Tao W, Zhu X, Yu X, Zeng X, Xiao Q, Zhang X, Ji X, Wang X, Shi J, Zhang H, Mei L. Adv Mater. 2017; 29:1603276.
87. Tarro G, Perna A, Esposito C. J Cell Physiol. 2005; 203:1. [PubMed: 15389637]
88. Morin PJ. Cancer Res. 2005; 65:9603. [PubMed: 16266975]
89. Kim J, Tung CH, Choi Y. Chem Commun. 2014; 50:10600.
90. Yuan Y, Zhang CJ, Gao M, Zhang R, Tang BZ, Liu Bin. Angew Chem Int Ed. 2015; 54:1780.
91. Cho Y, Kimz H, Choi Y. Chem Commun. 2013; 49:1202.
92. Huang Y, Song C, Li H, Zhang R, Jiang R, Liu X, Zhang G, Fan Q, Wang L, Huang W. ACS Appl Mater Interfaces. 2015; 7:21529. [PubMed: 26331442]
93. Shi H, Sun W, Liu C, Gu G, Ma B, Si W, Fu N, Zhang Q, Huang W, Dong X. J Mater Chem B. 2016; 4:113.
94. Gao S, Zhang L, Wang G, Yang K, Chen M, Tian R, Ma Q, Zhu L. Biomaterials. 2016; 79:36. [PubMed: 26691399]
95. Hu JJ, Liu LH, Li ZY, Zhuo RX, Zhang XZ. J Mater Chem B. 2016; 4:1932.
96. Shin WS, Lee MG, Verwilst P, Lee JH, Chi SG, Kim JS. Chem Sci. 2016; 7:6050.
97. Shin WS, Han J, Verwilst P, Kumar R, Kim JH, Kim JS. Bioconjug Chem. 2016; 27:1419. [PubMed: 27135737]
98. Liu P, Xu J, Yan D, Zhang P, Zeng F, Li B, Wu S. Chem Commun. 2015; 51:9567.
99. Wang YM, Wu Z, Liu SJ, Chu X. Anal Chem. 2015; 87:6470. [PubMed: 26044187]
100. Yuan Y, Kwok RTK, Tang BZ, Liu B. J Am Chem Soc. 2014; 136:2546. [PubMed: 24437551]
101. Li X, Mu J, Liu F, Tan EWP, Khezri B, Webster RD, Yeow EKL, Xing B. Bioconjug Chem. 2015; 26:955. [PubMed: 25938732]
102. Wang J, Zhang L, Chen M, Gao S, Zhu L. ACS Appl Mater Interfaces. 2015; 7:23248. [PubMed: 26388178]
103. Li SY, Cheng H, Xie BR, Qiu WX, Song LL, Zhuo RX, Zhang XZ. Biomaterials. 2016; 104:297. [PubMed: 27475726]
104. Jin CS, Cui L, Wang F, Chen J, Zheng G. Adv Healthc Mater. 2014; 3:1240. [PubMed: 24464930]
105. Zhang R, Feng G, Zhang CJ, Cai X, Cheng X, Liu B. Anal Chem. 2016; 88:4841. [PubMed: 27049534]
106. Schomburg I, Chang A, Placzek S, Söhngen C, Rother M, Lang M, Munaretto C, Ulas S, Stelzer M, Grote A, Scheer M, Schomburg D. Nucleic Acids Res. 2013; 41:D764. [PubMed: 23203881]
107. Decock J, Obermajer N, Vozelj S, Hendrickx W, Paridaens R, Kos J. Int J Biol Markers. 2008; 23:161. [PubMed: 18949742]
108. Lee GY, Qian WP, Wang L, Wang YA, Staley CA, Satpathy M, Nie S, Mao H, Yang L. ACS Nano. 2013; 7:2078. [PubMed: 23402593]
109. Whatcott CJ, Han H, Posner RG, Hostetter G, Von Hoff DD. Cancer Discovery. 2011; 1:291. [PubMed: 22053288]
110. Tan JX, Wang XY, Li HY, Su XL, Wang L, Ran L, Zheng K, Ren GS. Int J Cancer. 2011; 128:1303. [PubMed: 20473947]
111. Lokeshwar VB, Rubinowicz D, Schroeder GL, Forgacs E, Minna JD, Block NL, Nadji M, Lokeshwar BL. J Biol Chem. 2001; 276:11922. [PubMed: 11278412]
112. Egeblad M, Werb Z. Nat Rev Cancer. 2002; 2:161. [PubMed: 11990853]
113. Coussens LM, Fingleton B, Matrisian LM. Science. 2002; 295:2387. [PubMed: 11923519]
114. Danson S, Ward TH, Butler J, Ranson M. Cancer Treat Rev. 2004; 30:437. [PubMed: 15245776]
115. Cresteil T, Jaiswal AK. Biochem Pharmacol. 1991; 42:1021. [PubMed: 1651729]
116. Dinkova-Kostova AT, Talalay P. Arch Biochem Biophys. 2010; 501:116. [PubMed: 20361926]
117. Boudeau J, Miranda-Saavedra D, Barton GJ, Alessi DR. Trends Cell Biol. 2006; 16:443. [PubMed: 16879967]

118. Shin WS, Kwon J, Lee HW, Kang MC, Na HW, Lee ST, Park JH. Cancer Sci. 2013; 104:1120. [PubMed: 23663482]
119. Fan TJ, Han H, Cong S, Liang J. Acta Biochim Biophys Sin. 2005; 37:719. [PubMed: 16270150]
120. Chang Y, Yang L. Microbiol Mol Biol Rev. 2000; 64:821. [PubMed: 11104820]
121. Weitman SD, Lark RH, Coney LR, Fort DW, Frasca V, Zurawski VR Jr, Kamen BA. Cancer Res. 1992; 52:3396. [PubMed: 1596899]
122. Paulos CM, Turk MJ, Breur GJ, Low PS. Adv Drug Delivery Rev. 2004; 56:1205.
123. Hilgenbrink AR, Low PS. J Pharm Sci. 2005; 94:2135. [PubMed: 16136558]
124. Sudimack J, Lee RJ. Adv Drug Delivery Rev. 2000; 41:147.
125. Tros de Ilarduya C, Düzgünes N. Expert Opin Drug Delivery. 2013; 10:1583.
126. Tortorella S, Karagiannis TC. J Membr Biol. 2014; 247:291. [PubMed: 24573305]
127. Daniels TR, Delgado T, Helguera G, Penichet ML. Clin Immunol. 2006; 121:159. [PubMed: 16920030]
128. Gabathuler R. Neurobiol Dis. 2010; 37:48. [PubMed: 19664710]
129. Bildstein L, Dubernet C, Couvreur P. Adv Drug Delivery Rev. 2011; 63:3.
130. Leamon CP. Curr Opin Invest Drugs. 2008; 9:1277.
131. Russell-Jones G, McTavish K, McEwan J, Rice J, Nowotnik D. J Inorg Biochem. 2004; 98:1625. [PubMed: 15458825]
132. Mantovani A, Sozzani S, Locati M, Allavena P, Sica A. Trends Immunol. 2002; 23:549. [PubMed: 12401408]
133. Wu Y, Zheng L. Cancer Microenviron. 2012; 5:195. [PubMed: 22696271]
134. Carmeliet P. Nat Med. 2003; 9:653. [PubMed: 12778163]
135. Sharman WM, van Lier JE, Allen CM. Adv Drug Delivery Rev. 2004; 56:53.
136. David CJ, Chen M, Assanah M, Canoll P, Manley JL. Nature. 2010; 463:364. [PubMed: 20010808]
137. Chen T, Wu CS, Jimenez E, Zhu Z, Dajac JG, You M, Han D, Zhang X, Tan W. Angew Chem Int Ed. 2013; 52:2012.
138. Dong H, Dai W, Ju H, Lu H, Wang S, Xu L, Zhou SF, Zhang Y, Zhang X. ACS Appl Mater Interfaces. 2015; 7:11015. [PubMed: 25942410]
139. Wu D, Song G, Li Z, Zhang T, Wei W, Chen M, He X, Ma N. Chem Sci. 2015; 6:3839.
140. Ke K, Lin L, Liang H, Chen X, Han C, Li J, Yang HH. Chem Commun. 2015; 51:6800.
141. Qian RC, Cao Y, Long YT. Anal Chem. 2016; doi: 10.1021/acs.analchem.6b01804
142. Ding Q, Zhan Q, Zhou X, Zhang T, Xing D. small. 2016; doi: 10.1002/smll.201601724
143. Gao W, Cao W, Sun Y, Wei X, Xu K, Zhang H, Tang B. Biomaterials. 2015; 69:212. [PubMed: 26298289]
144. Dickinson BC, Chang CJ. Nat Chem Biol. 2011; 7:504. [PubMed: 21769097]
145. Lippert AR, De Bittner GCV, Chang CJ. Acc Chem Res. 2011; 44:793. [PubMed: 21834525]
146. Kim EJ, Bhuniya S, Lee H, Kim HM, Cheong C, Maiti S, Hong KS, Kim JS. J Am Chem Soc. 2014; 136:13888. [PubMed: 25238144]
147. Keisar OR, Ferber S, Fainaro RS, Shabat D. ChemMedChem. 2015; 10:999. [PubMed: 25847527]
148. Deng Z, Qian Y, Yu Y, Liu G, Hu J, Zhang G, Liu S. J Am Chem Soc. 2016; 138:10452. [PubMed: 27485779]
149. Fan W, Bu W, Shen B, He Q, Cui Z, Liu Y, Zheng X, Zhao K, Shi J. Adv Mater. 2015; 27:4155. [PubMed: 26058562]
150. Ma Z, Zhang M, Jia X, Bai J, Ruan Y, Wang C, Sun X, Jiang X. small. 2016; 12:5477. [PubMed: 27569525]
151. Cho S, Hwang O, Lee I, Lee G, Yoo D, Khang G, Kang PM, Lee D. Adv Funct Mater. 2012; 22:4038.
152. Kim H, Kim Y, Kim IH, Kim K, Choi Y. Theranostics. 2014; 4:1.

153. Yue C, Zhang C, Alfranca G, Yang Y, Jiang X, Yang Y, Pan F, Fuente JMdl, Cui D. Theranostics. 2016; 6:456. [PubMed: 26941840]
154. Yuan Y, Zhang CJ, Xua S, Liu B. Chem Sci. 2016; 7:1862.
155. Sies H. Free Radical Biol Med. 1999; 27:916. [PubMed: 10569624]
156. Gamcsik MP, Kasibhatla MS, Teeter SD, Colvin OM. Biomarkers. 2012; 17:671. [PubMed: 22900535]
157. Lee MH, Sessler JL, Kim JS. Acc Chem Res. 2015; 48:2935. [PubMed: 26513450]
158. Cho Y, Choi Y. Chem Commun. 2012; 48:9912.
159. Heo DN, Yang DH, Moon HJ, Lee JB, Bae MS, Lee SC, Lee WJ, Sun IC, Kwon IK. Biomaterials. 2012; 33:856. [PubMed: 22036101]
160. Bhuniya S, Maiti S, Kim EJ, Lee H, Sessler JL, Hong KS, Kim JS. Angew Chem Int Ed. 2014; 53:4469.
161. Wu X, Sun X, Guo Z, Tang J, Shen Y, James TD, Tian H, Zhu W. J Am Chem Soc. 2014; 136:3579. [PubMed: 24524232]
162. Turan IS, Cakmak FP, Yildirim DC, Atalay RC, Akkaya EU. Chem Eur J. 2014; 20:16088. [PubMed: 25345802]
163. He H, Lo PC, Ng DKP. Chem Eur J. 2014; 20:6241. [PubMed: 24737172]
164. Li L, Nurunnabi M, Nafiujjaman M, Jeong YY, Lee Yk, Huh KM. J Mater Chem B. 2014; 2:2929.
165. Zhao J, Huang L, Cui X, Li S, Wu H. J Mater Chem B. 2015; 3:9194.
166. Yuan Y, Zhang CJ, Kwok RTK, Xu S, Zhang R, Wu J, Tang BZ, Liu B. Adv Funct Mater. 2015; 25:6586.
167. Cao S, Pei Z, Xu Y, Pei Y. Chem Mater. 2016; 28:4501.
168. Fan H, Yan G, Zhao Z, Hu X, Zhang W, Liu H, Fu X, Fu T, Zhang XB, Tan W. Angew Chem Int Ed. 2016; 55:5477.
169. Yuan Y, Xu S, Zhang CJ, Zhang R, Liu B. J Mater Chem B. 2016; 4:169.
170. Kong F, Liang Z, Luan D, Liu X, Xu K, Tang B. Anal Chem. 2016; 88:6450. [PubMed: 27216623]
171. Tong H, Chen Y, Li Z, Li H, Chen T, Jin Q, Ji J. small. 2016; doi: 10.1002/smll.201601966
172. Ye M, Wang X, Tang J, Guo Z, Shen Y, Tian H, Zhu WH. Chem Sci. 2016; 7:4958.
173. Yuan Y, Xu S, Zhang CJ, Zhang R, Liu B. J Mater Chem B. 2016; 4:169.
174. Vaupel P, Schlenger K, Knoop C, Hçckel M. Cancer Res. 1991; 51:3316. [PubMed: 2040005]
175. Harris AL. Nat Rev Cancer. 2002; 2:38. [PubMed: 11902584]
176. Takasawa M, Moustafa RR, Baron JC. Stroke. 2008; 39:1629. [PubMed: 18369176]
177. Brown JM, Wilson WR. Nat Rev Cancer. 2004; 4:437. [PubMed: 15170446]
178. Feng W, Gao C, Liu W, Ren H, Wang C, Ge K, Li S, Zhou G, Li H, Wang S, Jia G, Li Z, Zhang J. Chem Commun. 2016; 52:9434.
179. Kumar R, Kim EJ, Han J, Lee H, Shin WS, Kim HM, Bhuniya S, Kim JS, Hong KS. Biomaterials. 2016; 104:119. [PubMed: 27449948]
180. Thambi T, Deepagan VG, Yoon HY, Han HS, Kimd SH, Son S, Jo DG, Ahn CH, Suh YD, Kim K, Kwon IC, Lee DS, Park JH. Biomaterials. 2014; 35:1735. [PubMed: 24290696]
181. Thambi T, Son S, Lee DS, Park JH. Acta Biomater. 2016; 29:261. [PubMed: 26472611]
182. Lin Q, Bao C, Yang Y, Liang Q, Zhang D, Cheng S, Zhu L. Adv Mater. 2013; 25:1981. [PubMed: 23401259]
183. Qian C, Yu J, Chen Y, Hu Q, Xiao X, Sun W, Wang C, Feng P, Shen QD, Gu Z. Adv Mater. 2016; 28:3313. [PubMed: 26948067]
184. Thambi T, Park JH, Lee DS. Chem Commun. 2016; 52:8492.
185. Gatenby RA, Gillies RJ. Nat Rev Cancer. 2004; 4:891. [PubMed: 15516961]
186. Gerweck LE, Seetharaman K. Cancer Res. 1996; 56:1194. [PubMed: 8640796]
187. Montcourrier P, Silver I, Farnoud R, Bird I, Rochefort H. Clin Exp Metastasis. 1997; 15:382. [PubMed: 9219726]

188. Park SY, Baik HJ, Oh YT, Oh KT, Youn YS, Lee ES. Angew Chem Int Ed. 2011; 50:1644.
189. Tian J, Ding L, Xu HJ, Shen Z, Ju H, Jia L, Bao L, Yu JS. J Am Chem Soc. 2013; 135:18850. [PubMed: 24294991]
190. Jung S, Nam J, Hwang S, Park J, Hur J, Im K, Park N, Kim S. Anal Chem. 2013; 85:7674. [PubMed: 23883363]
191. Wang C, Cheng L, Liu Y, Wang X, Ma X, Deng Z, Li Y, Liu Z. Adv Funct Mater. 2013; 23:3077.
192. Chen Y, Ye D, Wu M, Chen H, Zhang L, Shi J, Wang L. Adv Mater. 2014; 26:7019. [PubMed: 25156250]
193. Park D, Cho Y, Goh SH, Choi Y. Chem Commun. 2014; 50:15014.
194. Lee JY, Choi DY, Cho MY, Park KE, Lee SH, Cho SH, Hong KS, Lim YT. small. 2014; 10:901. [PubMed: 24106164]
195. Wu S, Han S, Han J, Su X. Chem Commun. 2014; 50:8014.
196. Zhou L, Chen Z, Dong K, Yin M, Ren J, Qu X. Biomaterials. 2014; 35:8694. [PubMed: 25002259]
197. Tian J, Ding L, Ju H, Yang Y, Li X, Shen Z, Zhu Z, Yu JS, Yang CJ. Angew Chem Int Ed. 2014; 53:9544.
198. Yu B, Li X, Zheng W, Feng Y, Wong YS, Chen T. J Mater Chem B. 2014; 2:5409.
199. Yuan Y, Kwok RTK, Tang BZ, Liu B. small. 2015; 11:4682. [PubMed: 26113312]
200. He L, Li Y, Tan CP, Ye RR, Chen MH, Cao JJ, Ji LN, Mao ZW. Chem Sci. 2015; 6:5409.
201. Tian J, Zhou J, Shen Z, Ding L, Yu JS, Ju H. Chem Sci. 2015; 6:5969.
202. Liu F, He X, Zhang J, Chen H, Zhang H, Wang Z. J Mater Chem B. 2015; 3:6731.
203. Hwang AA, Lu J, Tamanoi F, Zink JI. small. 2015; 11:319. [PubMed: 25196485]
204. Wang H, Di J, Sun Y, Fu J, Wei Z, Matsui H, Alonso AC, Zhou S. Adv Funct Mater. 2015; 25:5537.
205. Zhao Z, Wang X, Zhang Z, Zhang H, Liu H, Zhu X, Li H, Chi X, Yin Z, Gao J. ACS Nano. 2015; 9:2749. [PubMed: 25688714]
206. Liu F, He X, Chen H, Zhang J, Zhang H, Wang Z. Nat Commun. 2015; 6:8003. [PubMed: 26245151]
207. Guha S, Shaw GK, Mitcham TM, Bouchard RR, Smith BD. Chem Commun. 2016; 52:120.
208. Feng B, Zhou F, Xu Z, Wang T, Wang D, Liu J, Fu Y, Yin Q, Zhang Z, Yu H, Li Y. Adv Funct Mater. 2016; 26:7431.
209. Zhang Y, Teh C, Li M, Ang CY, Tan SY, Qu Q, Korzh V, Zhao Y. Chem Mater. 2016; 28:7039.
210. Dong Z, Feng L, Zhu W, Sun X, Gao M, Zhao H, Chao Y, Liu Z. Biomaterials. 2016; 110:60. [PubMed: 27710833]
211. Zhang J, Liu Z, Lian P, Qian J, Li X, Wang L, Fu W, Chen L, Wei X, Li C. Chem Sci. 2016; 7:5995.
212. Chen Y, Han H, Tong H, Chen T, Wang H, Ji J, Jin Q. ACS Appl Mater Interfaces. 2016; 8:21185. [PubMed: 27482632]
213. Lau JTF, Lo PC, Jiang XJ, Wang Q, Ng DKP. J Med Chem. 2014; 57:4088. [PubMed: 24793456]
214. Baek S, Singh RK, Kim TH, Seo Jw, Shin US, Chrzanowski W, Kim HW. ACS Appl Mater Interfaces. 2016; 8:8967. [PubMed: 26926826]
215. Mosaiab T, In I, Park SY. Macromol Rapid Commun. 2013; 34:1408. [PubMed: 23900997]
216. Li XS, Ke MR, Huang W, Ye CH, Huang JD. Chem Eur J. 2015; 21:3310. [PubMed: 25639348]
217. Ling D, Park W, Park S, Lu Y, Kim KS, Hackett MJ, Kim BH, Yim H, Jeon YS, Na K, Hyeon T. J Am Chem Soc. 2014; 136:5647. [PubMed: 24689550]
218. Wang T, Wang D, Yu H, Wang M, Liu J, Feng B, Zhou F, Yin Q, Zhang Z, Huang Y, Li Y. ACS Nano. 2016; 10:3496. [PubMed: 26866752]
219. Wang D, Wang T, Liu J, Yu H, Jiao S, Feng B, Zhou F, Fu Y, Yin Q, Zhang P, Zhang Z, Zhou Z, Li Y. Nano Lett. 2016; 16:5503. [PubMed: 27525587]
220. Cavani F, Trifro F, Vaccari A. Catal Today. 1991; 11:173.
221. Ladewig K, Xu ZP, Lu GQ. Expert Opin Drug Delivery. 2009; 6:907.

222. Choi SJ, Choy JH. Nanomedicine. 2011; 6:803. [PubMed: 21793673]
223. Shi J, Kantoff PW, Wooster R, Farokhzad OC. Nat Rev Cancer. 2017; 17:20. [PubMed: 27834398]

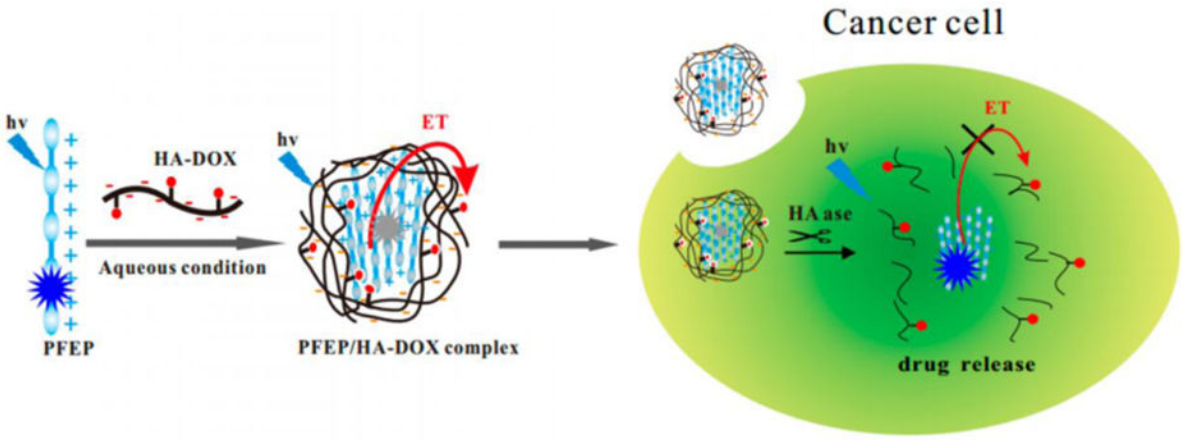

Figure 1.

Schematic illustration of a HAdase-activatable theranostic system. A cationic conjugated polymer (PFEP) forms a complex with hyaluronic acid (HA) conjugated with a drug (DOX). Electron transfer (ET) from PFEP to DOX occurs in this complex, leading to a quenched fluorescence emission. At the present of HAase in cancer cells, HA is degraded and DOX is released, resulting in the turn on signal of PFEP. Reproduced with permission.[92] Copyright 2015, American Chemical Society.

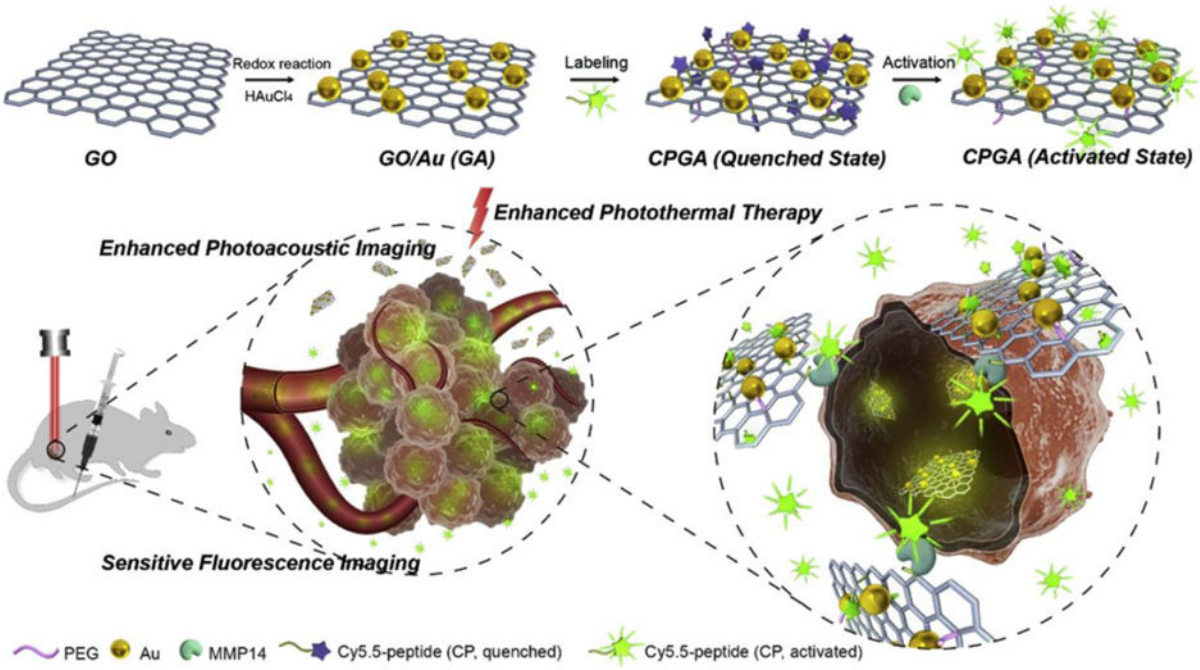

Figure 2.

Schematic illustration of a MMP-14 sensitive nanocomposite as multifunctional theranostic for both NIR FLI and PAI guided enhanced PTT. This theranostic agent is based on a graphene oxide (GO)-Au nanocomposite (GA) functionalized with an dye-labeled peptide (CP). Reproduced with permission.[94] Copyright 2016, Elsevier.

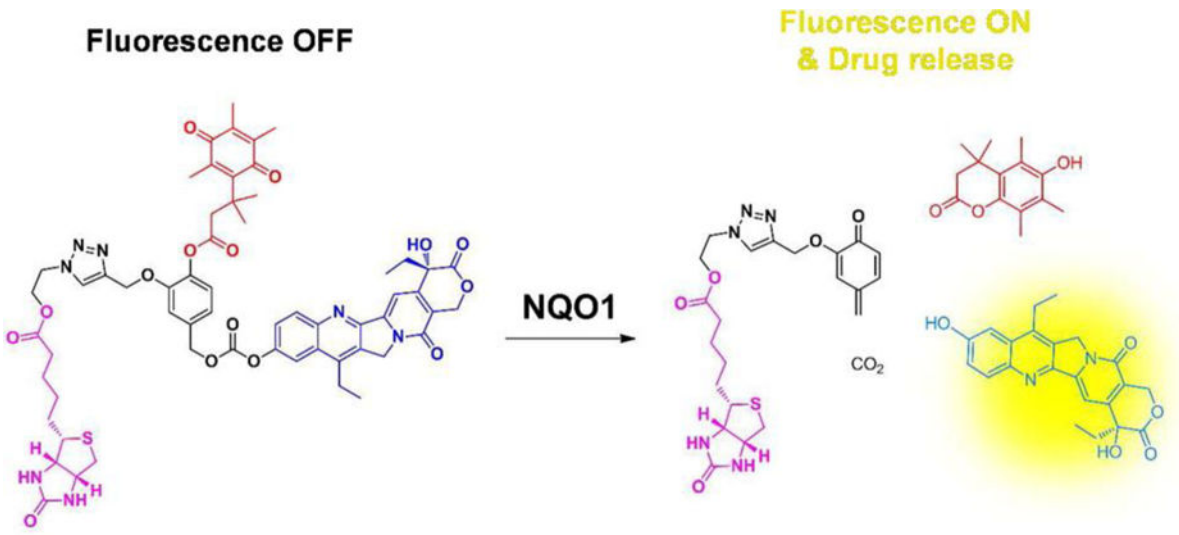

Figure 3.

Chemical structure and proposed mechanism of a NQO1 enzyme activatable theranostic prodrug system. Reproduced with permission.[97] Copyright 2016, American Chemical Society.

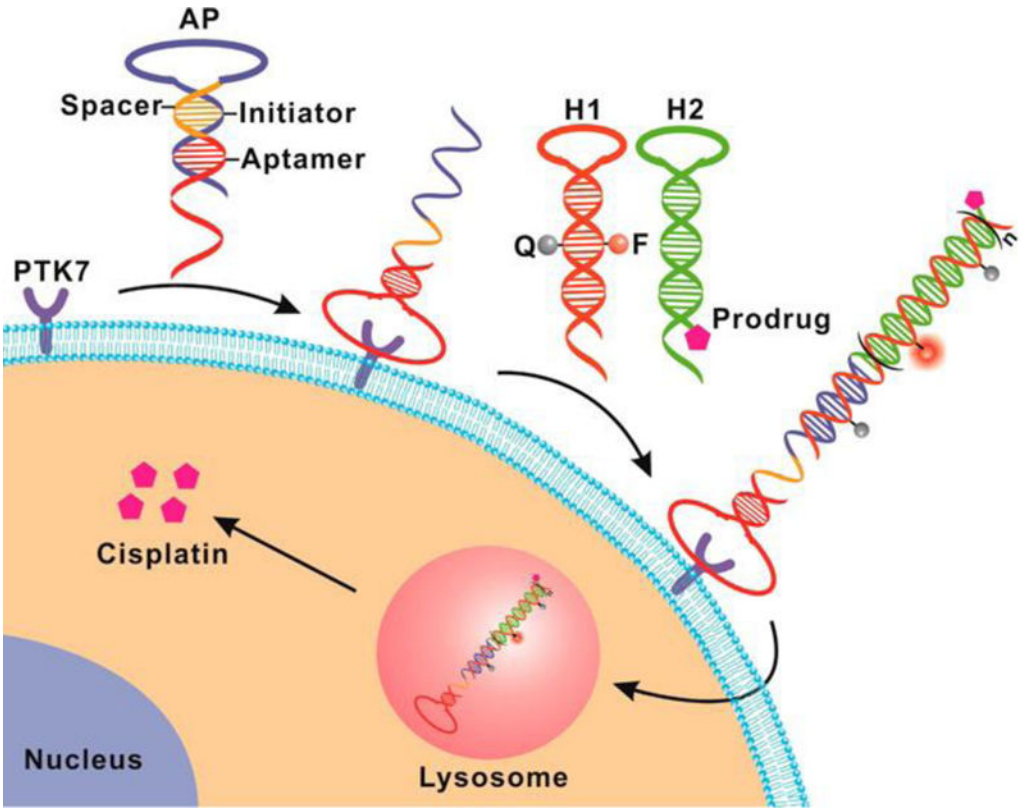

Figure 4.

Schematic illustration of structure-switching aptamer triggered hybridization chain reaction (SATHCR) approach to activatable theranostics. Reproduced with permission.[99] Copyright 2015, American Chemical Society.

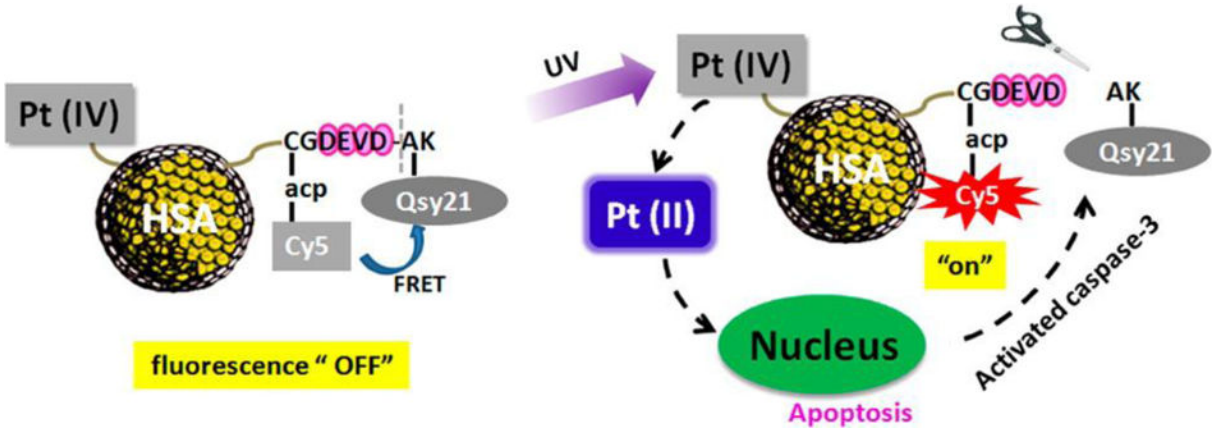

Figure 5.

Schematic illustration of caspase-3 activated theranostic systems for real-time monitoring of therapeutic agent induced apoptosis. Reproduced with permission.[101] Copyright 2015, American Chemical Society.

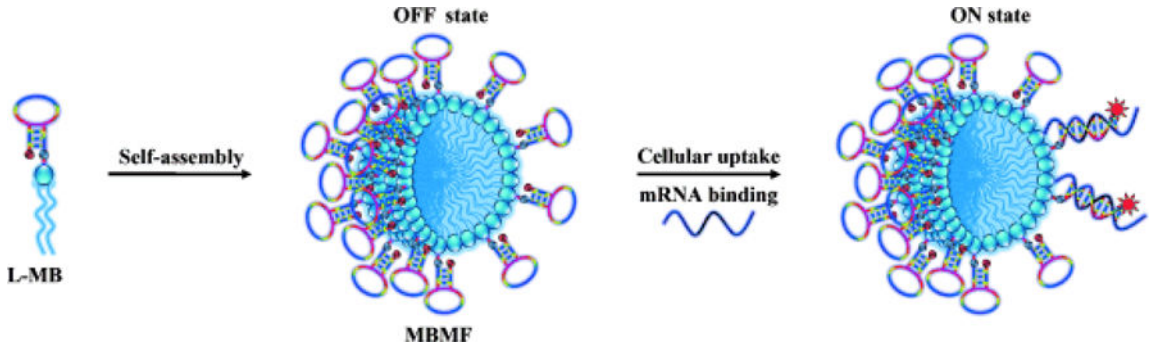

Figure 6.

Schematic illustration of a mRNA activatable theranostic system based on molecular beacon micelle flares (MBMFs) assembled by diacyllipid-molecular-beacon conjugates (L-MBs). Adapted with permission.[137] Copyright 2013, John Wiley and Sons.

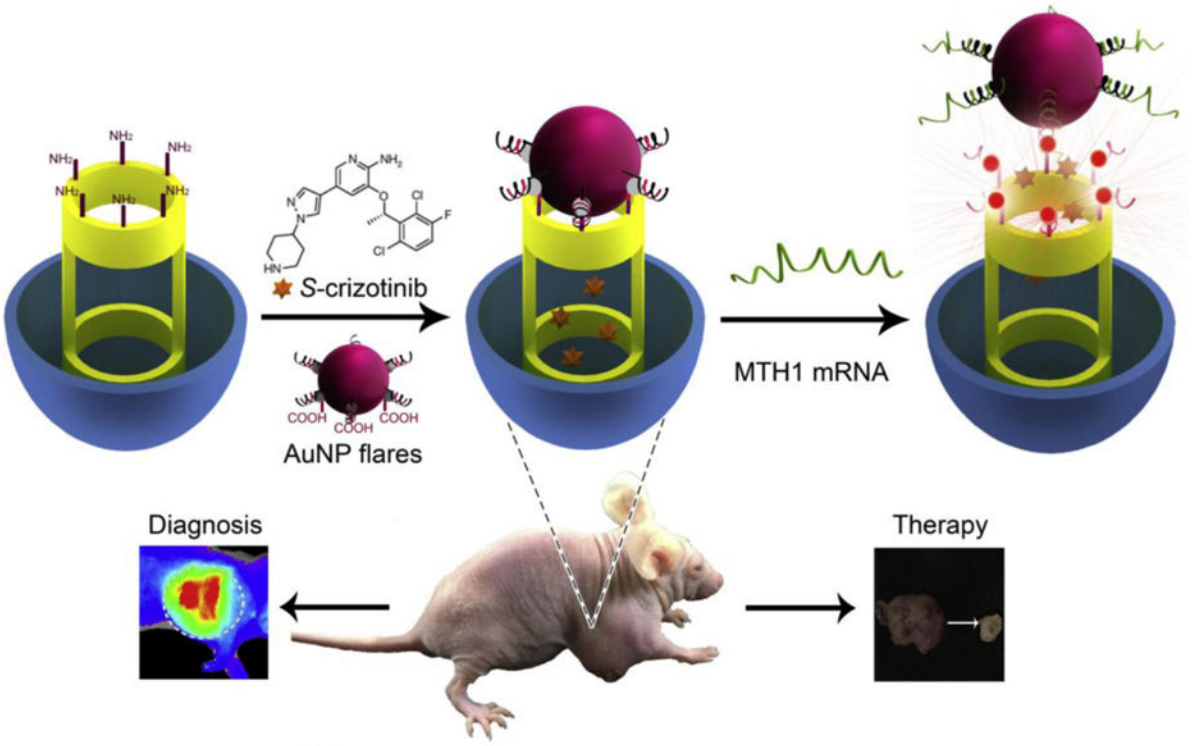

Figure 7.
Schematic illustration of a mRNA responsive gold nanoparticle (AuNP) flares-capped mesoporous silica nanoparticle (MSN) system. Reproduced with permission.[143] Copyright 2015, Elsevier.

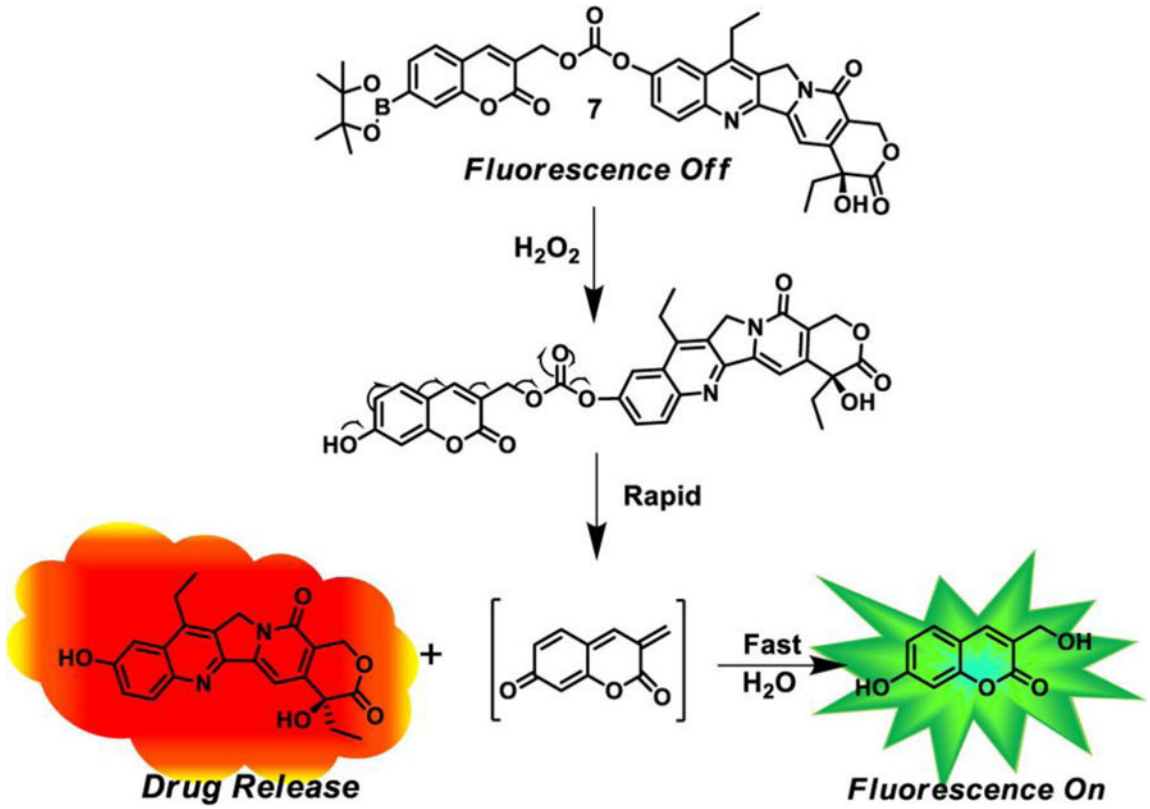

Figure 8.

Schematic illustration of a H_2O_2 activated prodrug. Reproduced with permission.[146] Copyright 2014, American Chemical Society.

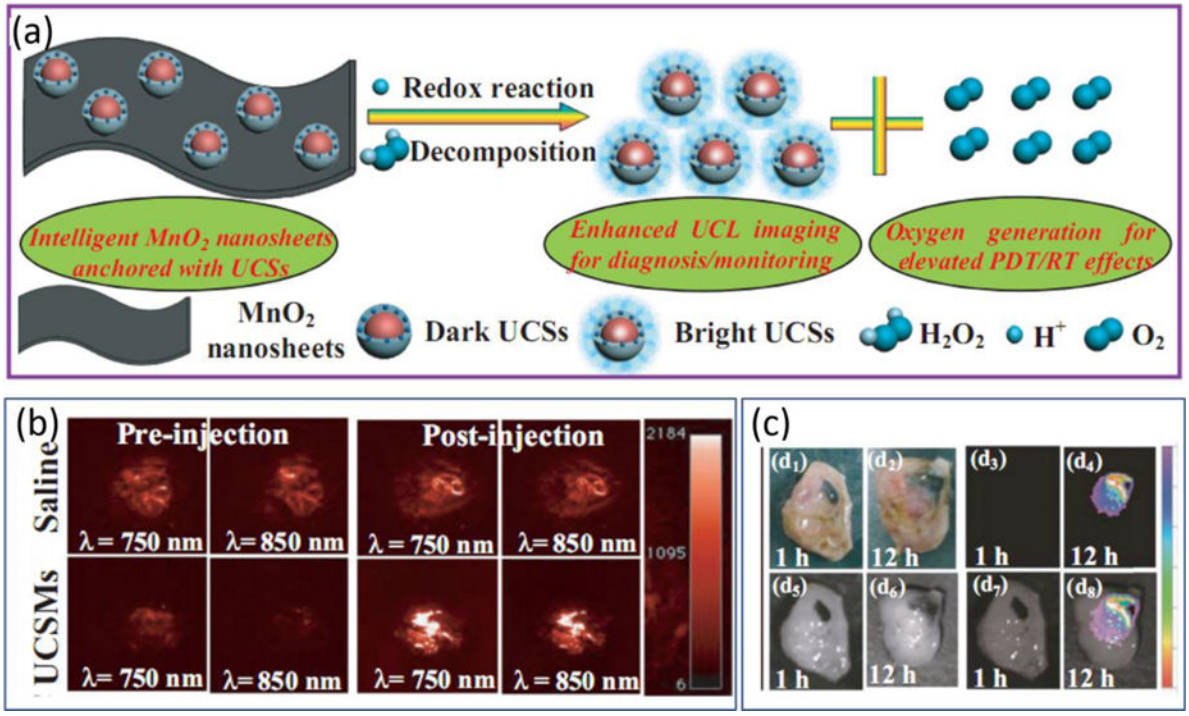

Figure 9.

Schematic illustration and results of studies of MnO_2 nanosheets-anchored with upconversion nanoprobes (UCSMs). (a) Decomposition of MnO_2 nanosheets triggered by the redox reaction between UCSMs and acidic H_2O_2, leading to the enhanced upconversion luminescent (UCL) imaging as well as the massive oxygen generation for improving the synergetic PDT/RT effects. (b) Representative 2D PAI of $4T_1$ solid tumors by measuring deoxygenated hemoglobin (λ = 750 nm) and oxygenated hemoglobin (λ = 850 nm) before/after injection of saline/UCSMs. (c) UCL imaging of 4T1 solid tumors at 1 and 12 h postinjection of UCSMs, respectively: $d_{1,2}$) digital photos; $d_{3,4}$) UCL imaging; $d_{5,6}$) bright field; $d_{7,8}$) mergence. Adapted with permission.[149] Copyright 2015, John Wiley and Sons.

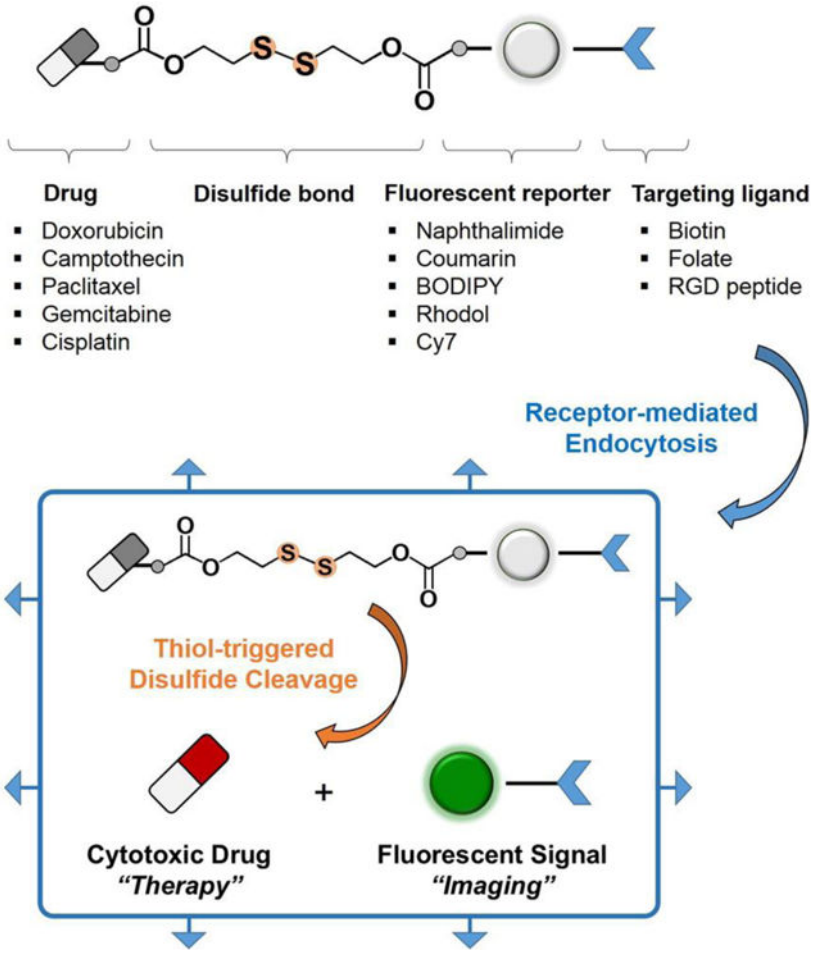

Figure 10.

Design elements of disulfide-based fluorescent drug conjugates. Reproduced with permission.[157] Copyright 2015, American Chemical Society.

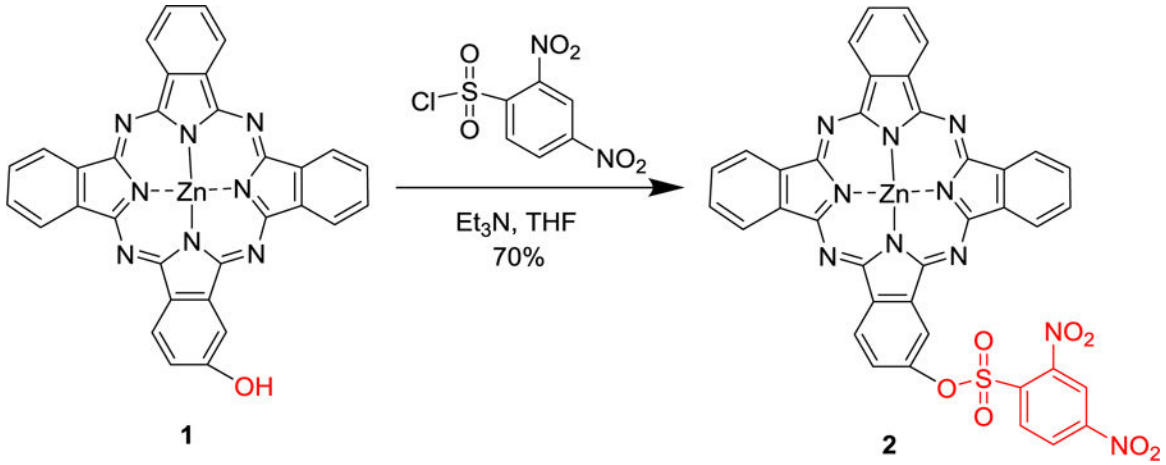

Figure 11.

Synthesis route of a GSH activatable phthalocyanine photosenisitizer. Adapted with permission.[163] Copyright 2014, John Wiley and Sons.

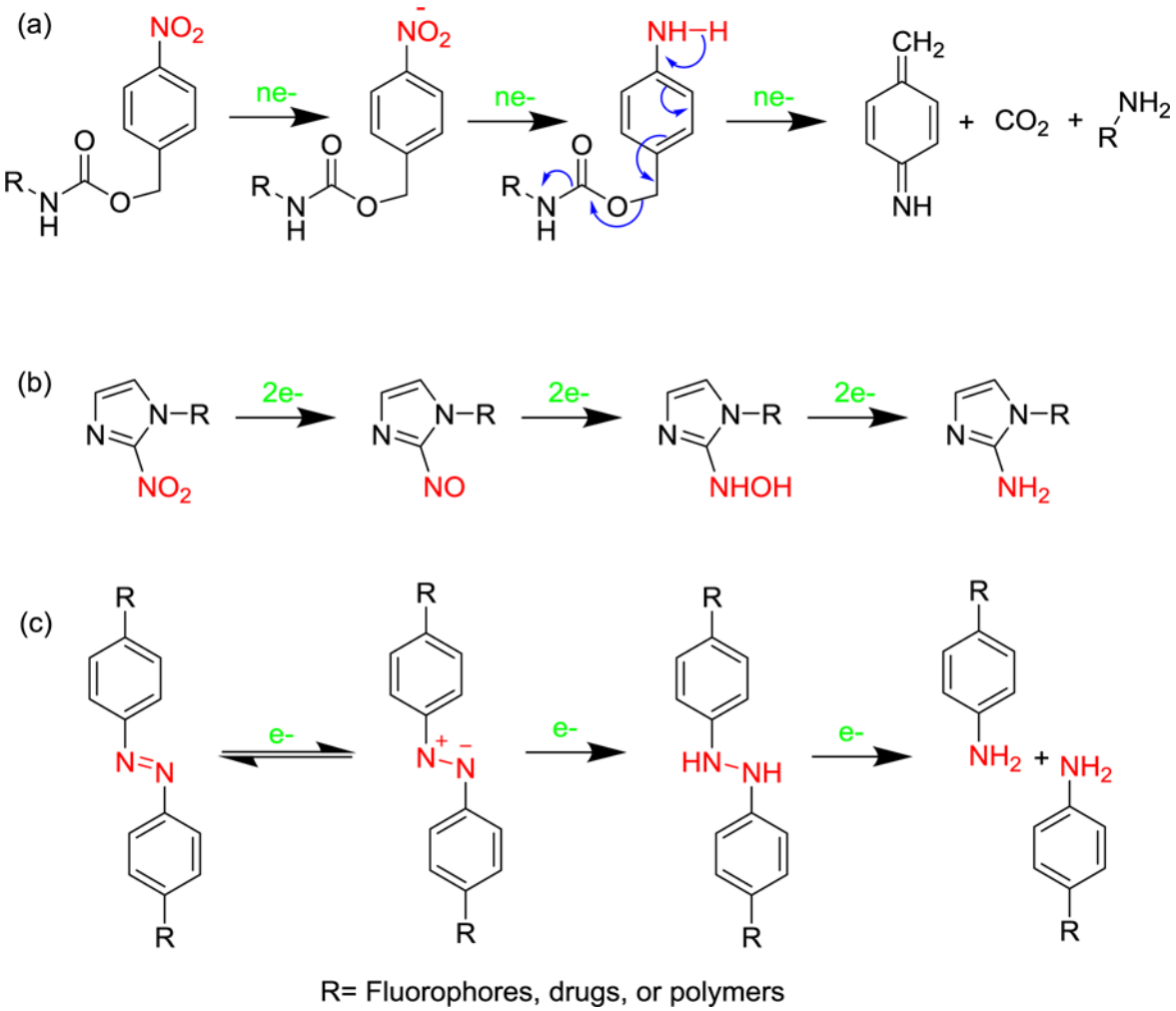

Figure 12.

Mechanism of hypoxic reduction of three representative responsive moieties: (a) nitrobenzyl alcohol, (b) nitroimidazole, and (c) azo derivatives.

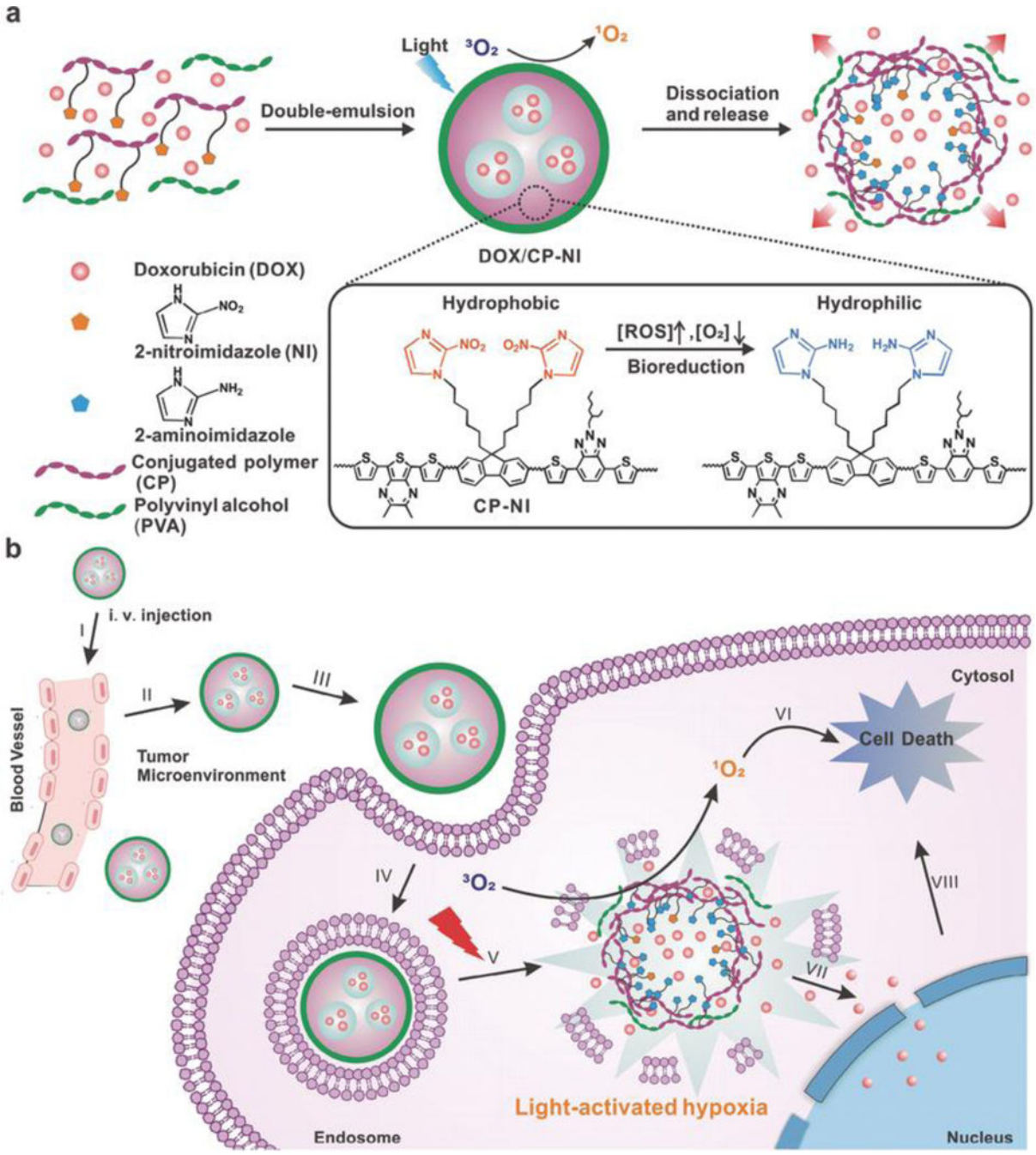

Figure 13.

Schematic illustration of a light and hypoxia responsive drug release system. Reproduced with permission.[183] Copyright 2016, John Wiley and Sons.

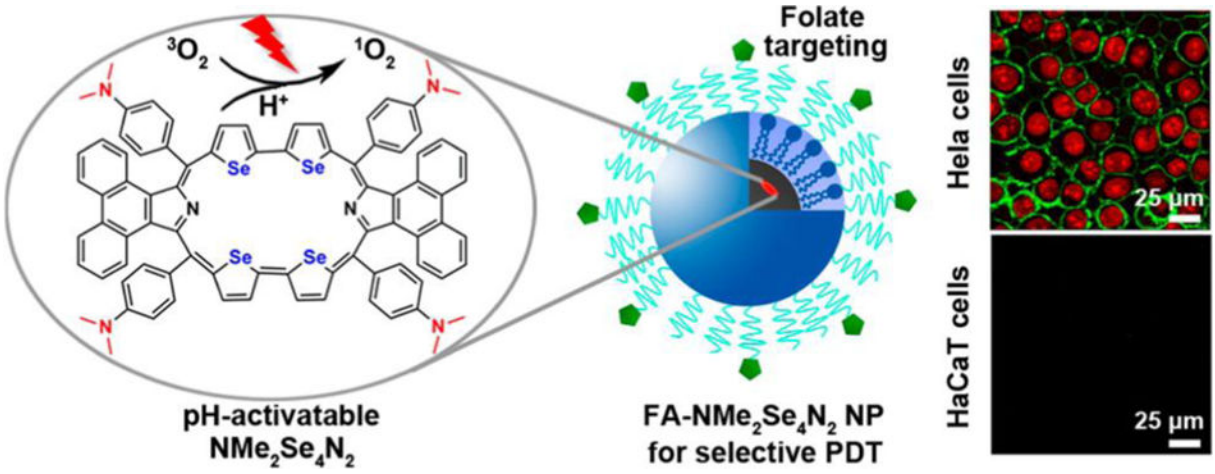

Figure 14.

Schematic illustrations of a pH-activatable selenium rubyrin-loaded nanosystem. Reproduced with permission.[189] Copyright 2013, American Chemical Society.

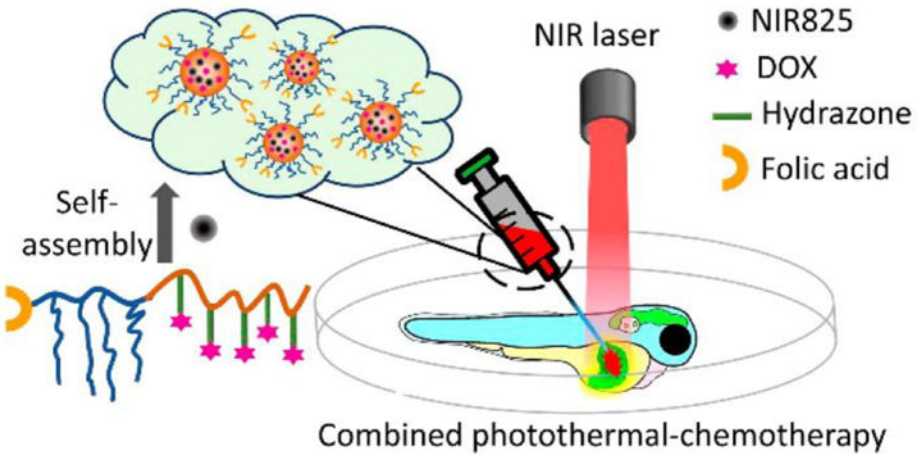

Figure 15.
Schematic illustration of a pH-activatable polymer-DOX-near infrared dye nanosystem. Reproduced with permission.[209] Copyright 2016, American Chemical Society.

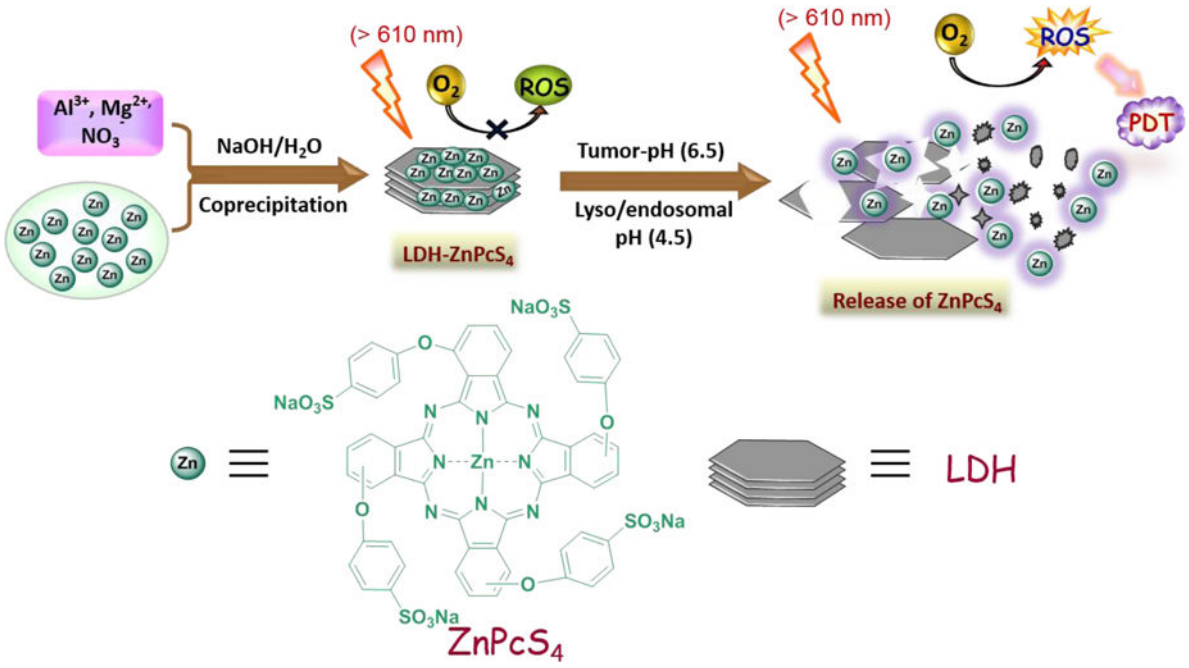

Figure 16.

Schematic illustration of a pH-activatable theranosticsystem based on acid sensitive layered double hydroxide (LDH). Adapted with permission.[216] Copyright 2015, John Wiley and Sons.

Table 1

Overview of imaging modalities.

Technology	Advantages	Disadvantages	Diagnosis in the clinic	Diagnosed tumor tissue in clinic
FLI	High sensitivity Multi-color detection Non-ionizing/Non-radioactive	Low spatial resolution Low tissue penetration	–	–
US	Low cost Fast diagnosis Non-ionizing/Non-radioactive	Low resolution Limited in organs containing gas or behind bones Depends on skilled operator	Pregnancy Cardiovascular diseases Thyroid-associated or lymphatic diseases Various Cancers	Thyroid, Breast, Pancreatic, Liver, Kidney, Prostate, Colorectal cancers
MRI	High spatial resolution Unlimited tissue penetration Non-ionizing/ Non-radioactive	Low sensitivity Time-consuming High cost	Bones and joints Tendon and ligament Cardiovascular disease Neuronal diseases Various cancers	Brain, Oral, Breast, Liver, Lung, Lymphoma, Kidney, Prostate, Colorectal cancers
CT	High spatial resolution Unlimited tissue penetration	Radiation risk	Bones and joints Brain diseases Lung diseases Various cancers	Brain, Oral, Thyroid, Breast, Pancreatic, Stomach, Liver, Lung, Lymphoma, Kidney, Prostate, Colorectal cancers
PET	High sensitivity Unlimited tissue penetration Quantitative	Radiation risk High cost	Neurological diseases Vascular diseases Infectious diseases Pharmacokinetics Various cancers	Brain, Oral, Thyroid, Breast, Pancreatic, Stomach, Liver, Lung, Lymphoma, Kidney, Prostate, Colorectal cancers
SPECT	High sensitivity Unlimited tissue penetration	Radiation risk Low spatial resolution	Bone Brain diseases Cardiovascular diseases Neurological diseases Various cancers	Brain, Oral, Thyroid, Breast, Pancreatic, Stomach, Liver, Lung, Lymphoma, Kidney, Prostate, Colorectal cancers
PAI	High spatial resolution Non-ionizing/Non-radioactive	Low sensitivity Low tissue penetration Limited in tissues blocked by bones or air cavities	–	–

Table 2

Protein-driven turn on theranostics.

Targeting protein	Bioactive link/group	Signal reporter	Therapeutic agent	Imaging modality	Therapeutic modality	Ref.
Cathepsin B	RRK	Ce4	Ce4	FLI	PDT	89
Cathepsin B	GFLG	AIEgen	AIEgen	FLI	PDT	90
HAase	HA	Ce6	GO/Ce6	FLI	PDT/PTT	91
HAase	HA	PEEP	DOX	FLI	CHT	92
HAase	HA	BODIPY	BODIPY	FLI	PDT	93
MMP-14	GATRLFGIRG	Cy5.5	GO/Au	FLI/PAI	PTT	94
MMP-2	GPLGVRGK	TAMRA	CPT	FLI	CHT	95
NQO1	Quinone	AIEgen	AIEgen	FLI	CHT	96
NQO1	Quinone	SN-38	SN-38	FLI	CHT	97
DT-diaphorase	Quinone	CPT	CPT	FLI	CHT	98
PTK7	sgc8	Cy5	Pt(IV)	FLI	CHT	99
Caspase-3	DEVD	AIEgen	Pt(IV)	FLI	CHT	100
Caspase-3	CGDEVDAK	Cy5	Pt(IV)	FLI	CHT	101
Caspase-3	GDEVDAPC	Cy5.5	ZnPc	FLI	PDT	102
Caspase-3	DEVD	FAM/PpIX	PpIX	FLI	PDT	103
FR	Folate	porphysome	porphysome	FLI	PDT	104
TfR	T7	AIEgen	AIEgen	FLI	PDT	105

Table 3

mRNA-driven turn on theranostics.

Bioactive link	Signal reporter	Therapeutic agent	Imaging modality	Therapeutic modality	Ref.
Hairpin DNA sequence	Rhodamine	MBMF	FLI	GT	137
Hairpin DNA sequence	MB	IP and ASODN	FLI	GT	138
Hairpin DNA sequence	TMB	Ce6	FLI	PDT	139
Hairpin DNA sequence	Cy3	Polypyrrole	FLI	PTT	140
Hairpin DNA sequence	Cy5	AuNPs	FLI	PTT	141
Hairpin DNA sequence	UCNPs	DOX	FLI	CHT	142
MTH1 mRNA sequence	Cy5	S-crizotinib	FLI	CHT	143

Table 4

ROS-driven turn on theranostics.

ROS	Bioactive link/group	Signal reporter	Therapeutic agent	Imaging modality	Therapeutic modality	Ref.
H_2O_2	Boronate	SN-38	SN-38	FLI	CHT	146
H_2O_2	Phenylboronic ester	QCy7	Camptothecin	FLI	CHT	147
H_2O_2	arylboronate ester	FITC/Gd	DOX	FLI/MRI	CHT	148
H_2O_2	MnO_2	UCSMs	MnO_2	UCLI/PAI	RT/PDT	149
H_2O_2	Fe^{3+}	Fe^{3+}	Methylene blue	MRI	PDT	150
H_2O_2	HPOX	Rubrene	HPOX	FLI	Antioxidant	151
$ONOO^-$	Hyaluronic acid	Ce6	Ce6	FLI	PDT	152
ROS	Thioketal	Ce6	CPT/Ce6	FLI	CHT/PDT	153
$^1O_2$	Aminoacrylate	AIEgen/Rho	AIEgen	FLI	PDT	154

Table 5

GSH-driven turn on theranostics.

Bioactive link/group	Signal reporter	Therapeutic agent	Imaging modality	Therapeutic modality	Ref.
S-S bond	Ce6	Ce6	FLI	PDT	158
S-Au bond	rhodamine B	paclitaxel	FLI	CHT	159
S-S bond	piperazine-rhodol	SN-38	FLI	CHT	160
S-S bond	dicyanomethylene-4H-pyran	CPT	FLI	CHT	161
Sulfonyl	BODIPY	BODIPY	FLI	PDT	162
Sulfonyl	ZnPc	ZnPc	FLI	PDT	163
S-Au bond	PhA	PhA	FLI	PDT	164
S-S bond	BODIPY	BODIPY	FLI	PDT	165
S-S bond	AIEgens	AIEgen	FLI	PDT	166
S-S bond	dicyanomethylene-4H-pyran	DOX	FLI	CHT	167
MnO_2	Ce6	Ce6	FLI	PDT	168
S-S bond	Ce4	Ce4	FLI	PDT	169
S-S bond	dicyanomethylene-4H-pyran	CPT	FLI	CHT	170
S-S bond	Ce6	Ce6	FLI	PDT	171
S-S bond	Cyanine/CPT	CPT	FLI	CHT	172
Sulfonyl	AIEgen	AIEgen	FLI	PDT	173

Table 6

Hypoxia-driven turn on theranostics.

Bioactive link/group	Signal reporter	Therapeutic agent	Imaging modality	Therapeutic modality	Ref.
4-nitrobenzyl	7-N,N-diethylaminocoumarin	Gemcitabine	FLI	CHT	178
4-nitrobenzyl	SN38	SN38	FLI	CHT	179
2-nitroimidazole	DOX	DOX	FLI	CHT	180
4-nitrobenzyl	DOX	DOX	FLI	CHT	181
2-nitroimidazole	7-aminocoumarin	Etoposide	FLI	CHT	182
2-nitroimidazole	DOX	DOX/CP-NI	FLI	CHT/PDT	183

Table 7

Slight acid-driven turn on theranostics.

pH of acid	Bioactive link/group	Signal reporter	Therapeutic agent	Imaging modality	Therapeutic modality	Ref.
6.8	Diethylaminopropyl	Ce6	Ce6	FLI	PDT	188
5.0	Dimethylaminophenyl	Rubyrin	Rubyrin	FLI	PDT	189
5.5	Ethylene amide	AuNPs	AuNPs	RAI	PTT	190
6.8	Dimethylmaleic acid	UCNP@2xCe6	UCNP@2xCe6	FLI	PDT	191
6.0	MnO_2	Mn^{2+}	DOX	MRI	CHT	192
5.0	DOX@HA	DOX	DOX	FLI	CHT	193
5.5	Diethylamino	BODIPY	Paclitaxel	FLI	CHT	194
5.0	PPy@SiO_2@dRB	dRB	PPy	FLI	PTT	195
4.5	Calcium phosphate	$NaGdF_4$:Ce/Tb	DOX	FLI/MRI	CHT	196
5.0	2-aminophenol	BDP-688	R16FP	FLI	PDT	197
5.3	Chitosan	CurP-SeNPs	CurP-SeNPs	FLI	CHT	198
5.0	Diisopropylamino	AIEgen/PheA	PheA	FLI	PDT	199
6.5	Imidazole	$Ir(NC)_2(NN)PF_6$	$Ir(NC)_2(NN)PF_6$	FLI	PDT	200
5.0	Diethylaminophenyl	BODIPY	BODIPY	FLI	PDT	201
6.5	Dopamine	Fe^{3+}	Polydopamine	MRI	PTT	202
6.0	Phenyl amine	DOX	DOX	FLI	CHT	203
5.8	Chitosan	DOX/CDs	DOX/CDs	FLI	CHT/PTT	204
5.4	MnAsOx complexes	Mn^{2+}	$HAsO_3^{2-}$	MRI	CHT	205
5.0	Fe^{3+}-gallic acid	Fe-CPNDs	Fe-CPNDs	MRI	PTT	206
6.5	Croconaine	Croconaine	Croconaine	PAI	PTT	207
6.2	Diamine	Ce6	HOT/Ce6	FLI	CHT/PDT	208
6.0	Hydrazone	IR825	DOX/ IR825	FLI	CHT/PTT	209
6.5	$CaCO_3$	Ce6(Mn)	Ce6(Mn)/DOX	MRI/FLI	CHT/PDT	210
6.2	Amine moiety	Hcyanine	Hcyanine	FLI	PTT	211
5.0	Hydrazone	AIEgen	DOX	FLI	CHT	212
6.0	Hydrazone	SiPc	SiPc	FLI	PDT	213
5.0	Amine	Au	DOX/Au	CT	CHT/PTT	214
5.0	Dimethylamino	BODIPY	DOX	FLI	CHT	215

pH of acid	Bioactive link/group	Signal reporter	Therapeutic agent	Imaging modality	Therapeutic modality	Ref.
6.5	LDH	ZnPc	ZnPc	FLI	PDT	216
6.8	Imidazole	Fe_3O_4/Ce6	Ce6	MRI/FLI	PDT	217
6.2	Tertiary amine	PDPA-Ce6/Gd^{3+}	PDPA-Ce6/DOX	FLI/PAI/MRI	PDT/PTT/CHT	218
6.2	Tertiary amine	PPa	PPa/SiRNA	FLI	PDT/Immunotherapy	219